

Multistep Oxidation of Diethynyl Oligophenylamine-Bridged Diruthenium and Diiron Complexes

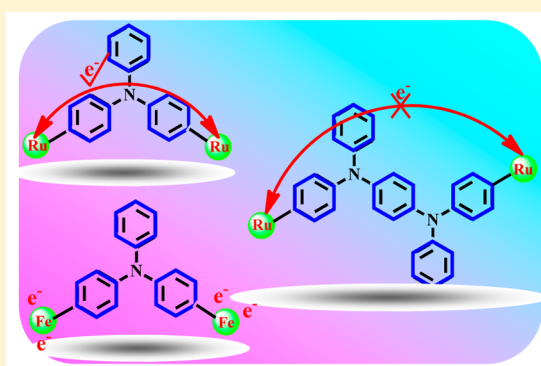
Jing Zhang,[†] Shen-Zhen Guo,[†] Yu-Bao Dong,[†] Li Rao,[†] Jun Yin,[†] Guang-Ao Yu,[†] František Hartl,^{*,‡,§} and Sheng Hua Liu^{*,†}

[†]Key Laboratory of Pesticide and Chemical Biology, Ministry of Education, College of Chemistry, Central China Normal University, Wuhan 430079, P. R. China

[‡]Department of Chemistry, University of Reading, Whiteknights, Reading RG6 6AD, U.K.

S Supporting Information

ABSTRACT: Homo-dinuclear nonlinear complexes $[\{M(\text{dppe})\text{-Cp}^*\}_2\{\mu\text{-}(-\text{C}\equiv\text{C})_2\text{X}\}]$ (dppe = 1,2-bis(diphenylphosphino)ethane; Cp* = $\eta^5\text{-C}_5\text{Me}_5$; X = triphenylamine (TPA), M = Ru (**1a**) and Fe (**1b**); X = *N,N,N',N'*-tetraphenylphenylene-1,4-diamine (TPPD), M = Ru (**2a**)) were prepared and characterized by ^1H , ^{13}C , and ^{31}P NMR spectroscopy and single-crystal X-ray diffraction (**1a**, **2a**). Attempts to prepare the di-iron analogue of **2a** were not successful. Experimental data obtained from cyclic voltammetry, square wave voltammetry, UV–vis–NIR (NIR = near-infrared) spectro-electrochemistry, and very informative IR spectro-electrochemistry in the $\text{C}\equiv\text{C}$ stretching region, combined with density functional theory calculations, afford to make an emphasizing assessment of the close association between the metal–ethynyl termini and the oligophenylamine bridge core as well as their respective involvement in sequential one-electron oxidations of these complexes. The anodic behavior of the homo-bimetallic complexes depends strongly both on the metal center and the length of the oligophenylamine bridge core. The poorly separated first two oxidations of di-iron complex **1b** are localized on the electronically nearly independent Fe termini. In contrast, diruthenium complex **1a** exhibits a significantly delocalized character and a marked electronic communication between the ruthenium centers through the diethynyl–TPA bridge. The ruthenium–ethynyl halves in **2a**, separated by the doubly extended and more flexible TPPD bridge core, show a lower degree of electronic coupling, resulting in close-lying first two anodic waves and the NIR electronic absorption of $[\mathbf{2a}]^+$ with an indistinctive intervalence charge transfer character. Finally, the third anodic waves in the voltammetric responses of the homo-bimetallic complexes are associated with the concurrent exclusive oxidation of the TPA or TPPD bridge cores.



INTRODUCTION

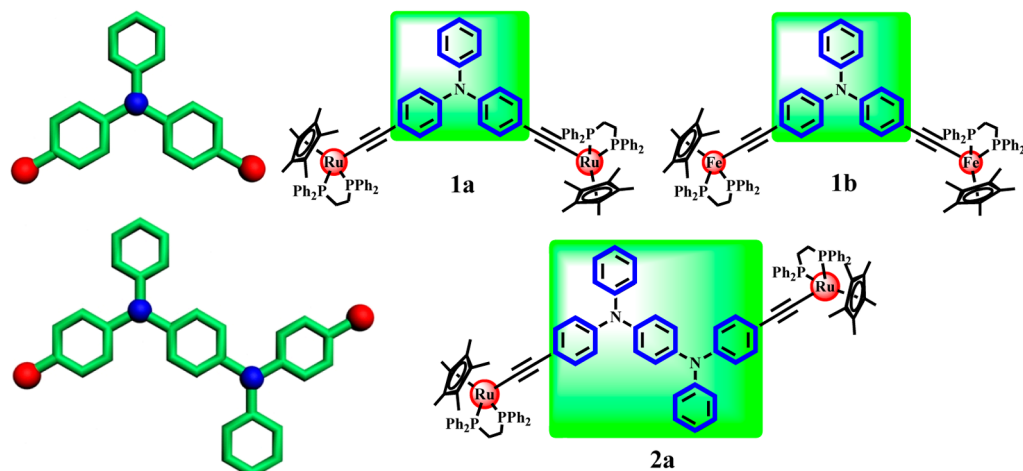
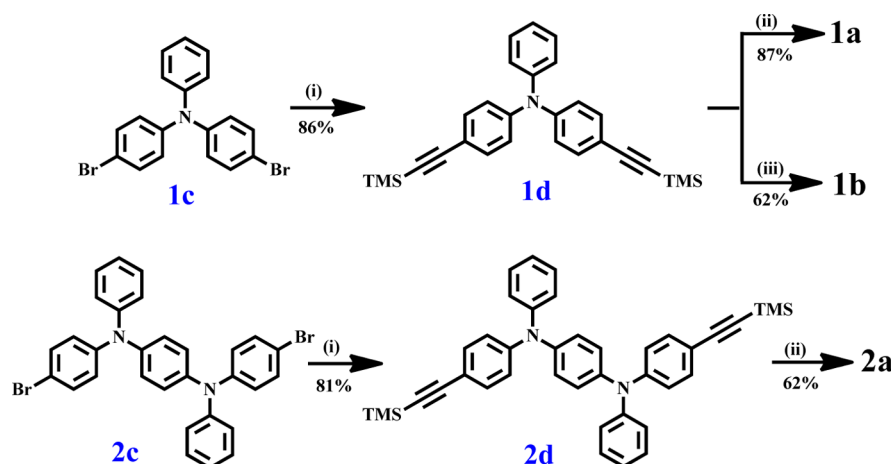
In recent years mixed-valence (MV) states of binuclear complexes have attracted considerable attention,^{1,2} providing important model systems for intramolecular charge transfer processes and offering broad prospects for building highly functionalized molecules with interesting electronic and optoelectronic properties essential for molecular scale electroactive materials and devices.^{3–6} In this respect, numerous studies focused in the past decades on rigid and π -conjugated bridging ligands connecting two redox-active metallic termini, as the simplest models for the electron-transfer phenomena in the MV systems.^{7–10} Comprehensive studies have explored a wide range of systems designed to provide some insight into electron transfer over a long distance.¹¹ However, increasing the chain length to a modest degree decreased significantly solubility of the prototypical π -conjugated systems in common organic solvents, and the complexity of their syntheses essentially arose. These factors present obstacles for the relevant fundamental research and restrict the longitudinal extension and processability in electronic devices.¹¹ In this

respect, continued search for novel or modified perspective systems to eliminate the above-mentioned drawbacks is very meaningful and challenging.

Triphenylamine (TPA) and other mono- and oligomeric triarylamine derivatives have widely been used as selective one-electron reductants, electrocatalysts, and hole-transporting materials in organic optoelectronic devices, such as photoconductors, photorefractive materials, and organic light-emitting devices. This is ascribed to their favorable redox properties, with one or more readily accessible oxidations and high stabilities of the corresponding radical cations with appropriate substitution patterns.^{12–14} Moreover, TPA has also been considered as an ideal redox center to study the intermolecular electron transfer processes in MV systems.^{15–17} Despite the efforts, reports on mixed-valence systems featuring the TPA unit as (a component of) a bridging ligand are relatively limited in number compared with the π -conjugated

Received: November 23, 2016

Chart 1. Studied Diethynyl Oligophenylamine-Bridged Homo-Bimetallic Ruthenium and Iron Complexes

Scheme 1. General Synthetic Routes to Complexes 1a, 1b, and 2a^a

^aReagents and conditions: (i) [Pd(PPh₃)₄], CuI, Et₃N, TMSA, in THF; (ii) [RuCl(dppe)Cp*], KF, MeOH/THF; (iii) K₂CO₃ in CH₃OH, [FeCl(dppe)Cp*], NaBPh₄, *t*-BuOK.

68 systems,¹⁸ let alone a detailed discussion of their electronic
69 properties.^{18d} In another aspect, a nonrigid TPA-based
70 structure with appropriate substituents^{12–14} offers a viable
71 solution to the problem of poorly soluble elongated systems
72 and the difficulty in synthesizing large dendrimers. Notably,
73 Onitsuka and co-workers synthesized successfully a series of
74 ruthenium–acetylide dendrimers with the tris(4-
75 ethynylphenyl)amine bridging ligand up to the second
76 generation by using a convergent method.¹⁸ⁱ In this work we
77 focus on TPA and scarcely reported tetraphenylphenylenedi-
78 amine (TPPD) in the core of the diethynyl-terminated bridge.
79 The external “Ru(dppe)Cp*” and “Fe(dppe)Cp*” (dppe = 1,2-
80 bis(diphenylphosphino)ethane; Cp* = η⁵-C₅Me₅) units com-
81 pleting the studied homo-bimetallic chains (Chart 1) are
82 particularly suited as reference redox-active termini in
83 molecular wire models to study their MV properties, as
84 documented by the previously reported work.^{2d–h,19} The
85 assembly of multiple redox-active components was anticipated
86 to exhibit peculiar electrochemical and photophysical proper-
87 ties. Hereinafter we detail our efforts to explore to which degree
88 the redox, spectroscopic, and bonding properties and electronic
89 communication in the investigated homo-bimetallic series are
90 affected by the varied combination of the oligophenylamine

bridge core and the metal centers. The input data for the
91 discussion have been obtained by using controlled-potential
92 voltammetry and UV–vis–NIR/IR (NIR = near-infrared)
93 spectro-electrochemistry combined with density functional
94 theory (DFT) calculations.
95

RESULTS AND DISCUSSION

Syntheses and Characterization. The general synthetic
97 route to homo-dinuclear metal complexes 1a, 1b, and 2a is
98 outlined in Scheme 1. Bridge precursors 1d and 2d were
99 obtained in yields higher than 80%, having used Pd/Cu-
100 catalyzed Sonogashira coupling reactions between 4-bromo-*N*-
101 (4-bromophenyl)-*N*-phenylaniline (1c), *N*¹,*N*⁴-bis(4-bromo-
102 phenyl)-*N*¹,*N*⁴-diphenylbenzene-1,4-diamine (2c), and tri-
103 methylsilylacetylene (TMSA), respectively. Subsequently, the
104 trimethylsilyl (TMS) termini in compounds 1d and 2d were
105 deprotected with KF or K₂CO₃ to give the terminal bis(alkyne)
106 and then reacted with [RuCl(dppe)Cp*] and [FeCl(dppe)-
107 Cp*] to obtain the corresponding target complexes 1a, 2a, and
108 1b, respectively. Unfortunately, deprotected 2d did not
109 coordinate to the Fe(dppe)Cp* termini by this procedure,²⁰
110 and the intended diethynyl-TPPD diiron complex (2b) was not
111 obtained. Notably, no obvious differences have been observed
112

113 in comparative NMR responses of related diruthenium
114 complexes **1a** and **2a**, specifically, the dppe signals in the ^1H
115 and ^{31}P NMR spectra and the Ru–C \equiv C signals in the ^{13}C
116 NMR spectra.

117 **X-ray Crystallography.** The molecular structures of solid
118 **1a** and **2a** were resolved by single-crystal X-ray diffraction.
119 Pertinent diffraction parameters are given in Table S1 (see the
120 [Supporting Information](#)). Important bond lengths (Å), bond
121 angles (deg), and Ru...Ru distances (Å) in the crystal structures
122 are collected in [Table 1](#). The structures of **1a** and **2a** feature

Table 1. Selected Bond Lengths (Å), Angles (deg), and Inter-Ruthenium Distances (Å) in the Crystal Structures of Complexes 1a and 2a

complex 1a			
Ru(1)–C(37)	1.999 (3)	C(43)–C(44)	1.378 (4)
Ru(1)–P(1,2)	2.250 (9), 2.258 (8)	C(39)–C(44)	1.395 (5)
C(37)–C(38)	1.209 (4)	C(45)–C(46)	1.384 (4)
C(38)–C(39)	1.436 (4)	C(46)–C(47)	1.378 (5)
C(39)–C(40)	1.401 (5)	C(47)–C(48)	1.371 (5)
C(40)–C(41)	1.382 (4)	N(1)–C(42)	1.426 (3)
C(41)–C(42)	1.387 (4)	N(1)–C(45)	1.403 (5)
C(42)–C(43)	1.391 (4)	Ru(1)...Ru(2)	14.19
P(1)–Ru(1)–P(2)			83.3 (3)
Ru(1)–C(37)–C(38)			174.9 (3)
C(37)–C(38)–C(39)			175.6 (3)
complex 2a			
Ru(1)–C(27)	1.991 (5)	C(36)–C(37)	1.343 (2)
Ru(1)–P(1,2)	2.246 (3), 2.248 (3)	C(37)–C(38)	1.390 (2)
C(27)–C(28)	1.214 (9)	C(38)–C(39)	1.394 (2)
C(28)–C(29)	1.448 (7)	C(39)–C(40)	1.348 (2)
C(29)–C(30)	1.375 (9)	C(35)–C(40)	1.402 (8)
C(30)–C(31)	1.360 (8)	C(41)–C(42)	1.363 (9)
C(31)–C(32)	1.390 (9)	C(42)–C(43)	1.393 (9)
C(32)–C(33)	1.378 (9)	C(41)–C(43)	1.390 (8)
C(33)–C(34)	1.389 (7)	N(1)–C(32)	1.428 (5)
C(29)–C(34)	1.392 (2)	N(1)–C(41)	1.424 (6)
C(35)–C(36)	1.392 (2)	Ru(1)...Ru(2)	20.68
P(1)–Ru(1)–P(2)			84.4 (3)
Ru(1)–C(37)–C(38)			178.5 (3)
C(37)–C(38)–C(39)			176.1 (3)

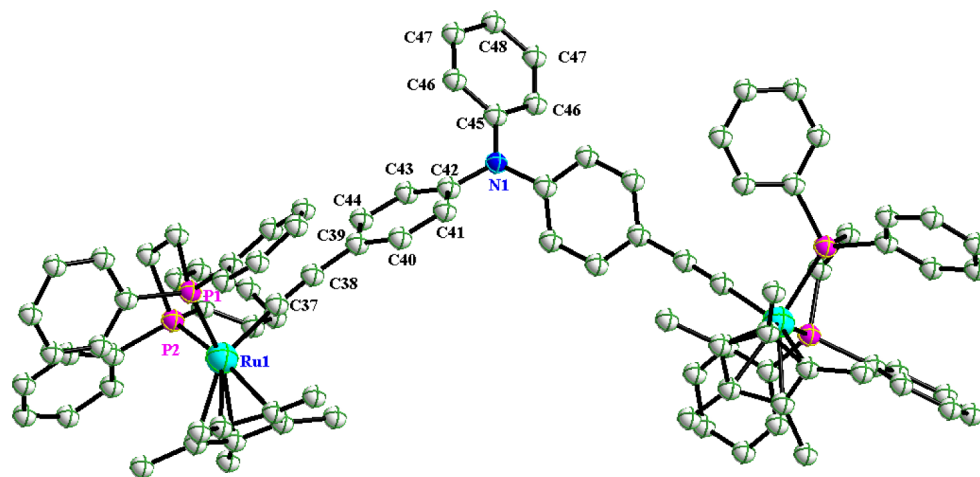


Figure 1. X-ray crystal structure of **1a** shown with thermal ellipsoids at the 50% probability level. Hydrogen atoms were omitted for clarity. Full crystallographic details are given in [Supporting Information](#). CCDC No. 1435472.

123 approximately linear Ru–C \equiv C–C moieties, the pairs of Ru–
124 C \equiv C and C \equiv C–C angles being 174.9°, 175.6° and 178.5°,
125 176.1°, respectively. As seen in [Figure 1](#) and [Figure S1\(A\)](#)
126 ([Supporting Information](#)), the crystallographic analysis mani-
127 fests typical pseudo-octahedral geometry around the ruthenium
128 centers. The C \equiv C bond lengths [1.209 Å (**1a**) and 1.214 Å
129 (**2a**)] comply with a carbon–carbon triple bond, and the
130 bonding parameters of the Ru(dppe)Cp* group, including the
131 Ru–C and Ru–P distances and P–Ru–P angles, compare well
132 with the data reported for a range of similar systems.^{21,22}
133 Elongation of the bridging ligand core from monoamine (TPA)
134 in **1a** to diamine (TPPD) in **2a** caused the Ru(1)...Ru(2)
135 distance to increase considerably from 14.19 to 20.68 Å. These
136 data are consistent with the corresponding calculated results
137 presented hereinafter.

138 Some additional interesting features can be found in the
139 crystal packing ([Figure S1\(B\)](#)). Complex **2a** shows typical
140 lamellar packing characteristics with the parallel arrangements
141 of the bridge and metallic termini in each layer from the side
142 view of the lamellar structure, the benzene rings 1, 3 and 2, 4 of
143 the diamine bridge core ([Figure S1\(B\)](#)) being oriented in
144 opposite directions and arranged in parallel with each other.

Electrochemical Properties. The anodic behavior of
145 complexes **1a**, **1b**, and **2a** was investigated by cyclic
146 voltammetry (CV) and square-wave voltammetry (SWV) in
147 deaerated dichloromethane containing 1×10^{-1} M *n*-Bu₄NPF₆
148 as the supporting electrolyte ([Figure 2](#)). The TMS-terminated
149 precursors **1d** and **2d** ([Scheme 1](#)) were also studied for
150 comparison (see [Supporting Information](#), [Figure S2](#)). The
151 relevant electrochemical data are summarized in [Table 2](#).
152

153 Complexes **1a** and **1b** exhibit three successive oxidation
154 steps. The anodic behavior of **2a** is more complex, and only the
155 first four anodic processes were investigated. Comparing the
156 electrochemical behavior of diruthenium complexes **1a** and **2a**,
157 the potentials of their first three anodic steps ($E_{1/2}(1,2,3)$) are
158 similar. The main difference arises in the wave splitting
159 $\Delta E_{1/2}(1-2)$ and the thermodynamic stability (comproportion-
160 ation) constant K_c of $[\mathbf{2a}]^+$, which is considerably smaller than
161 that determined for $[\mathbf{1a}]^+$ ([Table 2](#)). This result has likely its
162 origin in the extended bridge core in **2a** and limited electronic
163 communication between two redox active Ru–C \equiv C units,
164 resembling in this respect an earlier reported series of 164

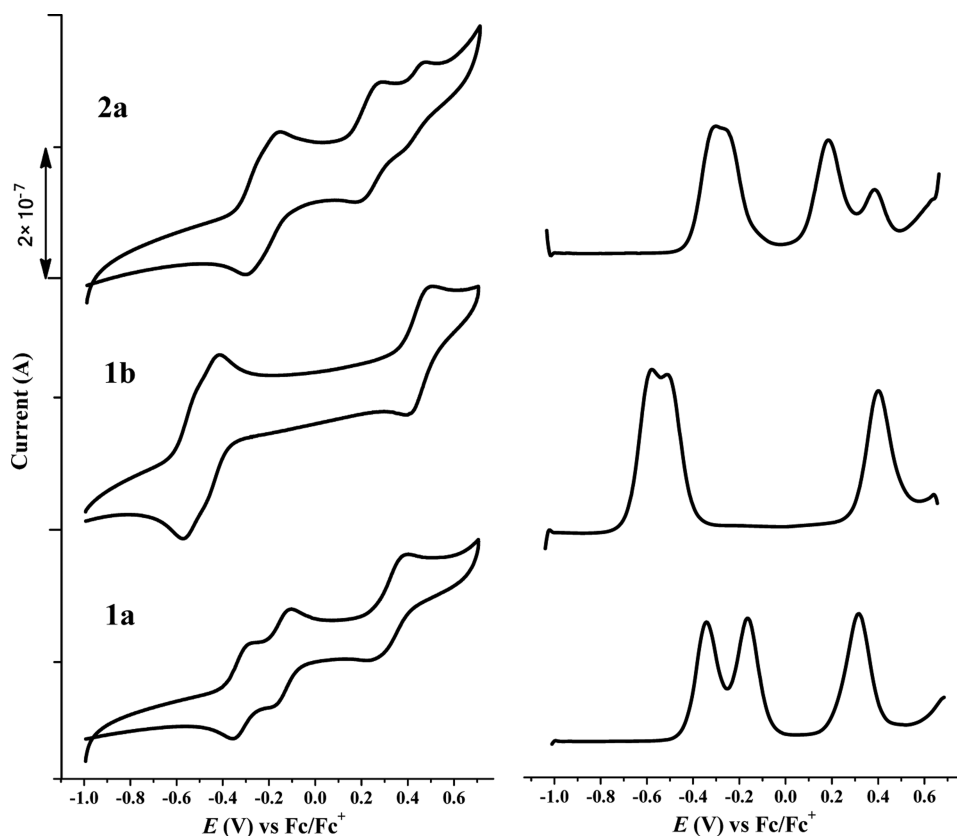


Figure 2. (left) CV of complexes **1a**, **1b**, and **2a** in $\text{CH}_2\text{Cl}_2/n\text{-Bu}_4\text{NPF}_6$ at $\nu = 50 \text{ mV s}^{-1}$. (right) Corresponding SWV of complexes **1a**, **1b**, and **2a** at $f = 10 \text{ Hz}$ and $t_p = 25 \text{ mV}$.

Table 2. Electrochemical Data for Complexes **1a**, **1b**, and **2a**, TMS-Terminated Reference Compounds **1d** and **2d**, a Dinuclear Vinyl–Ruthenium Complex Related to **1a**, and Reference Phenylamines^a

compound	$E_{1/2}(1)$ (V)	$E_{1/2}(2)$ (V)	$E_{1/2}(3)$ (V)	$E_{1/2}(4)$ (V)	$\Delta E_{1/2}(1-2)$ (mV)	K_c^b
1a	-0.36	-0.18	0.30		180	1.1×10^3
Ru–vinyl ^c	-0.17	0.15	0.59		320	3.8×10^5
1b	-0.56	-0.50	0.41		60	10
1d	0.66					
TPA ^d	0.70 ^{e,f}					
2a	-0.31	-0.26	0.19	0.39	50	7
2d	0.21	0.68				
TPPD ^d	0.14 ^f	0.63				

^aThe anodic potentials are referenced against the standard ferrocene/ferrocenium (Fc/Fc^+) redox couple. ^bThe comproportionation constants K_c were estimated using the expression $K_c = \exp(\Delta E/25.69 \text{ mV})$ at 298 K, with input data recorded at $\nu = 50 \text{ mV s}^{-1}$. ^c $[\text{Cl}(\text{CO})(\text{P}(\text{t}r_3)\text{Ru}-\text{CH}=\text{CH}-\text{C}_6\text{H}_4-\text{N}(\text{C}_6\text{H}_4\text{OCH}_3)_2)]$. ^dReference 18f. ^eIrreversible anodic peak potential. ^fPotential determined against an Ag/AgCl reference electrode; $E_{1/2}(\text{Fc}/\text{Fc}^+) = +0.43 \text{ V}$ versus Ag/AgCl .

165 oligothiophene-bridged diruthenium diethynyl complexes.²¹
 166 The additional fourth anodic wave of **2a** at a higher potential
 167 can safely be ascribed to the second oxidation of the diamine
 168 core, based on comparison with the anodic potentials of the
 169 TMS-terminated diethynyl TPPD reference compound **2d**.

170 The obvious difference in the composition of **1a** and **1b** is
 171 the metallic redox center. Interestingly, the replacement of
 172 ruthenium in **1a** with iron in **1b** resulted in a slightly negative
 173 shift of the first anodic wave (at $E_{1/2}(1)$) and significantly
 174 decreased comproportionation constant K_c (Table 2). It will be
 175 shown in the spectro-electrochemical section that the formally
 176 Fe(II) centers in the terminal positions of **1b** oxidize in a more
 177 localized fashion compared to the Ru(II) derivative, **1a**, as also
 178 encountered in the literature for related compounds.^{3c,8b,18h,23}

Accordingly, the two formally Fe(II) centers in **1b** 179
 communicate poorly through the twisted ethynyl–phenyl- 180
 ene–N–phenylene–ethynyl bridge, in line with the small 181
 $\Delta E_{1/2}(1-2)$ and K_c values for **[1b]⁺**. Consequently, it was 182
 hardly possible to record IR and UV–vis–NIR spectra of 183
 “pure” **[1b]⁺** in the course of the corresponding spectro- 184
 electrochemical experiments described in the following section. 185
 A less severe restriction applies in this regard for **[2a]⁺**. 186

A significantly greater involvement of the TPA core in the 187
 electrochemical oxidation has been reported^{18d} for a bridged 188
 dinuclear vinyl–ruthenium complex, causing a stronger 189
 electronic interaction between the ruthenium–vinyl linker 190
 subunits in the corresponding one-electron oxidized cation and 191
 a larger K_c value (Table 2). The different auxiliary ligands at the 192

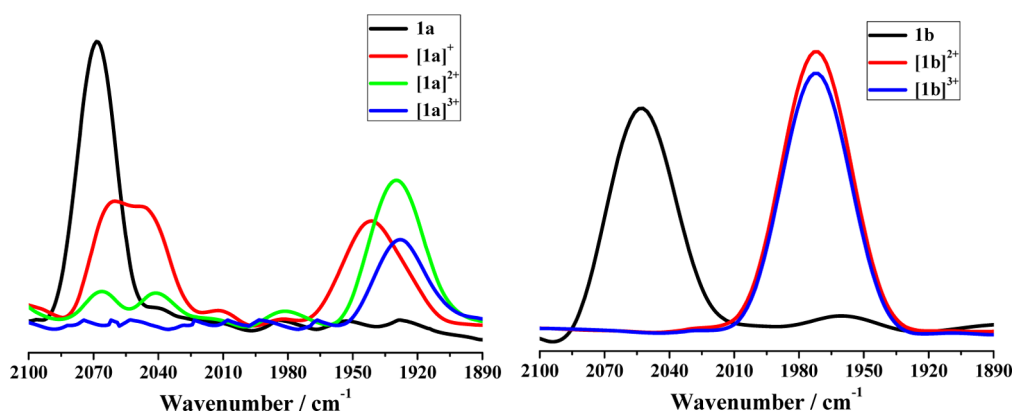


Figure 3. IR spectra recorded in the $\nu(\text{C}\equiv\text{C})$ region for complexes **1a** and **1b** in different oxidation states generated in $\text{CH}_2\text{Cl}_2/1 \times 10^{-1} \text{ M } n\text{-Bu}_4\text{NPF}_6$ at 298 K within an OTTLE cell. For the chemical oxidation of **1b** to $[\text{1b}]^+$ see Supporting Information, Figure S6.

193 ruthenium center, specifically, *trans*- $\text{RuCl}(\text{CO})\{\text{P}(i\text{-Pr})_3\}_2$, also
 194 play a role in the control of the electronic conjugation between
 195 the TPA bridge core and the ruthenium–linker (vinyl vs
 196 ethynyl) subunits. For example, smaller differences in the
 197 anodic behavior exist between TPA-based mono- and trinuclear
 198 vinyl–ruthenium^{18d} and ethynyl–ruthenium²⁴ complexes with
 199 similar ruthenium coordination sites.

200 **IR and UV–vis–NIR Spectro-Electrochemistry.** IR and
 201 UV–vis–NIR spectro-electrochemical studies were undertaken
 202 to get insight into the nature of the physical and electronic
 203 structures in different oxidation states within the investigated
 204 three redox series.

205 The IR spectra of neutral complexes **1a**, **1b**, and **2a** are
 206 characterized by a strong single $\nu(\text{C}\equiv\text{C})$ band (Figure 3,
 207 Figure S3 (Supporting Information), and Table 3). By contrast,

individual ethynyl–ruthenium moieties in the oxidation
 217 process.

218
 The second anodic step toward $[\text{1a}]^{2+}$ led to the
 219 disappearance of both $\nu(\text{C}\equiv\text{C})$ bands close to the wave-
 220 number of the neutral parent state, while a new single band at
 221 1930 cm^{-1} gained intensity. This behavior suggests the
 222 complete oxidation of both $\text{Ru}-\text{C}\equiv\text{C}$ centers in $[\text{1a}]^{2+}$.
 223 Importantly, no prominent low-energy shift of the $\nu(\text{C}\equiv\text{C})$
 224 mode was observed for the subsequent anodic generation of the
 225 tricationic product $[\text{1a}]^{3+}$, characterized by a single absorption
 226 band marking a symmetric electronic structure. The very little
 227 $\nu(\text{C}\equiv\text{C})$ shift compares well with the invariable $\nu(\text{C}\equiv\text{C})$
 228 wavenumber encountered for the TMS-terminated diethynyl
 229 TPA reference $[\text{1d}]$ and its monocation (Supporting
 230 Information, Figure S4), suggesting the dominantly TPA-
 231 localized one-electron oxidation of $[\text{1a}]^{2+}$.
 232

The anodic conversion of **2a** to $[\text{2a}]^{2+}$ was marked by
 233 gradual disappearance of the parent $\nu(\text{C}\equiv\text{C})$ absorption at
 234 2068 cm^{-1} and the growth of a new absorption band at 1934
 235 cm^{-1} belonging to the dication (Supporting Information,
 236 Figure S3). The red shift of 134 cm^{-1} is close to that of 138
 237 cm^{-1} observed for the oxidation of **1a** to $[\text{1a}]^{2+}$ (Table 3),
 238 indicating comparable participation of the ethynyl linkers in the
 239 oxidation of **2a** to the symmetric dication, in line with the
 240 theoretical description (see below). The small separation of the
 241 first two anodic waves of **2a** implies that singly oxidized $[\text{2a}]^+$
 242 can hardly be observed in the pure form. The IR spectrum in
 243 Figure S3 corresponding to the redox equilibrium with the
 244 highest concentration of $[\text{2a}]^+$ was selected with the aid of the
 245 characteristic NIR electronic absorption of the monocation (see
 246 below) simultaneously monitored in the course of the careful
 247 anodic electrolysis within the OTTLE cell. It can safely be
 248 concluded that $[\text{2a}]^+$ exists only in a single conformation
 249 detectable on the time scale inherent to IR spectroscopy,
 250 differently from $[\text{1a}]^+$ (see above). The IR $\nu(\text{C}\equiv\text{C})$
 251 absorption of $[\text{2a}]^+$ overlaps with those of parent **2a** and
 252 ultimately $[\text{2a}]^{2+}$ (Table 3), rendering the monocation with
 253 weak electronic coupling between the $\text{Ru}-\text{C}\equiv\text{C}$ termini not
 254 exceeding that in $[\text{1a}]^+$, in line with the corresponding CV
 255 responses (Table 2).
 256

The third anodic step producing stable $[\text{2a}]^{3+}$ was not
 257 accompanied by any $\nu(\text{C}\equiv\text{C})$ shift, causing merely a strongly
 258 diminished intensity of the $\nu(\text{C}\equiv\text{C})$ band at 1934 cm^{-1}
 259 (Figure S3). This behavior reflects the dominant oxidation of
 260 the TPPD bridge core in $[\text{2a}]^{2+}$ to the corresponding radical
 261 cation. This assignment is supported by the invariable $\nu(\text{C}\equiv\text{C})$
 262

Table 3. Spectro-Electrochemically Determined $\nu(\text{C}\equiv\text{C})$ Wavenumbers (cm^{-1}) for $[\text{1a}]^{n+}$, $[\text{1b}]^{n+}$, $[\text{1d}]^{n+}$ and $[\text{2a}]^{n+}$, $[\text{2d}]^{n+}$

complex	$n = 0$	$n = 1$	$n = 2$	$n = 3$	$n = 4$
$[\text{1a}]^{n+}$	2068 (s)	2059 (m), 2046 (m), 1941 (m)	1930 (m)	1928 (w- m)	
$[\text{1b}]^{n+}$	2052 (s)	<i>a</i>	1972 (s)	1972 (s)	
$[\text{1d}]^{n+}$	2065	2065			
$[\text{2a}]^{n+}$	2068 (s)	2066, 1935 ^b	1934 (s)	1933 (w)	<i>c</i>
$[\text{2d}]^{n+}$	2066 (m)	2066 (m)	2066 (s)		

^aThe $\nu(\text{C}\equiv\text{C})$ absorption of $[\text{1b}]^+$ is not reported due to the small K_c value and a low conversion evidenced by UV–vis–NIR spectroscopy (Supporting Information, Figure S6). ^bThis absorption does not correspond to the pure form of $[\text{2a}]^+$ due to small K_c but to the maximum conversion reached by electrochemical oxidation of **2a** determined by parallel UV–vis–NIR monitoring (Supporting Information, Figure S12). ^cNo $\nu(\text{C}\equiv\text{C})$ band perceptible.

208 the $\nu(\text{C}\equiv\text{C})$ pattern of one-electron-oxidized $[\text{1a}]^+$ is more
 209 complex, consisting of a strongly shifted, fairly broad, and
 210 slightly asymmetric absorption band at 1941 cm^{-1} and two
 211 overlapping $\nu(\text{C}\equiv\text{C})$ bands at 2059 and 2046 cm^{-1} , that is,
 212 near the absorption of parent **1a** at 2068 cm^{-1} . These spectral
 213 changes comply with the presence of a symmetry-broken
 214 radical cation $[\text{1a}]^+$ on the time scale of IR spectroscopy ($1 \times$
 215 10^{-11} to $1 \times 10^{-12} \text{ s}$), existing in different conformations
 216 (rotamers)²⁵ with slightly different participation of the

263 wavenumber in the TMS-terminated reference redox series
 264 $[2d]^{n+}$ ($n = 0, 1, 2$); see Table 3 and Supporting Information,
 265 Figure S4.

266 The poorly resolved first two anodic steps of **1b** (Table 2 and
 267 Figure 2) resemble the oxidation of **2a**. We note that the $\nu(\text{C}\equiv\text{C})$
 268 shift induced by the oxidation of **1b** to $[\mathbf{1b}]^{2+}$ is merely 80
 269 cm^{-1} compared to 134 cm^{-1} for $2a \rightarrow [2a]^{2+}$, and 138 cm^{-1} for
 270 $1a \rightarrow [1a]^{2+}$ featuring the same molecular bridge (Table 3). This
 271 difference points to significantly more Fe-centered oxidation of
 272 the Fe–C \equiv C termini, as also confirmed by DFT calculations
 273 (see below). The electronic interaction between the Fe centers
 274 in $[\mathbf{1b}]^+$ through the TPA core becomes strongly limited,
 275 resulting in dominant disproportionation of the monocation to
 276 **1b** and $[\mathbf{1b}]^{2+}$. Therefore, $[\mathbf{1b}]^+$ is hardly detectable by IR
 277 spectroscopy (Table 3 and Supporting Information, Figures S5
 278 and S6), and only the characteristic NIR absorption
 279 (Supporting Information, Figure S6) reveals its presence. The
 280 negligible change in the $\nu(\text{C}\equiv\text{C})$ wavenumber accompanying
 281 the third anodic step producing $[\mathbf{1b}]^{3+}$ resembles the formation
 282 of $[\mathbf{1a}]^{3+}$ (Figure 3), both bearing the TPA-core oxidation
 283 characteristics.

284 The UV–vis–NIR spectra of complexes **1a**, **1b**, and **2a** and
 285 TMS-terminated bridges **1d** and **2d** in the different oxidation
 286 states were recorded by using the spectro-electrochemical
 287 monitoring or stepwise chemical oxidation, as shown in Figures
 288 4 and 5 and Supporting Information, Figures S7–S12. The
 289 relevant data are collected in Table 4.

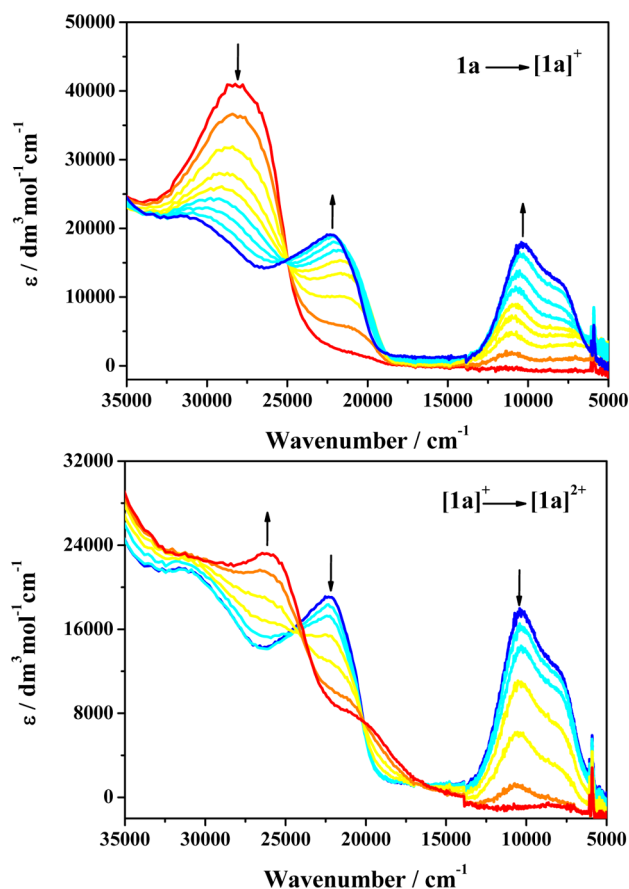


Figure 4. UV–vis–NIR spectral changes recorded during the oxidation of complex **1a** to $[\mathbf{1a}]^+$ (top) and $[\mathbf{1a}]^{2+}$ (bottom) in $\text{CH}_2\text{Cl}_2/1 \times 10^{-1} \text{ M } n\text{-Bu}_4\text{NPF}_6$ at 298 K within an OTTLE cell.

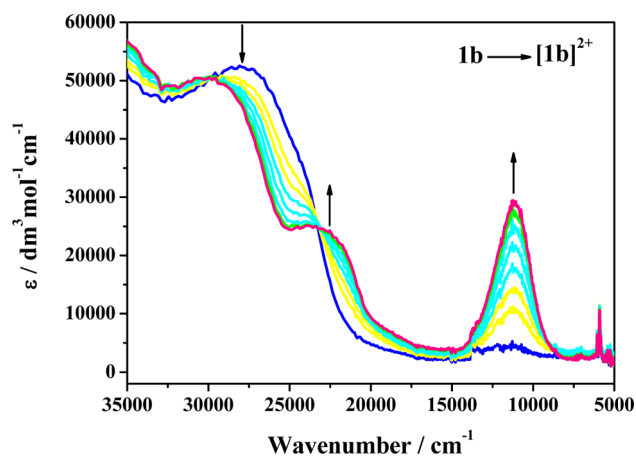


Figure 5. UV–vis–NIR spectral changes recorded during the oxidation of complex **1b** to $[\mathbf{1b}]^{2+}$ in $\text{CH}_2\text{Cl}_2/1 \times 10^{-1} \text{ M } n\text{-Bu}_4\text{NPF}_6$ at 298 K within an OTTLE cell.

Table 4. UV–Vis–NIR Electronic Absorption of Complexes **1a**, **1b**, **1d**, **2a**, **2d**, and Their Oxidized Forms in Dichloromethane/ $n\text{-Bu}_4\text{NPF}_6$

complex	$\bar{\nu}_{\text{max}}$ (cm^{-1}) (ϵ_{max} ($\text{dm}^3 \text{mol}^{-1} \text{cm}^{-1}$))
1a	28 100 (41 300)
$[\mathbf{1a}]^+$	22 200 (19 500), 10 200 (18 100), 7800 (12 400)
$[\mathbf{1a}]^{2+}$	26 000 (23 300), 20 500 (7600)
$[\mathbf{1a}]^{3+}$	23 800 (21 900), 8300 (10 400)
1b	27 500 (52 700)
$[\mathbf{1b}]^+$	^a
$[\mathbf{1b}]^{2+}$	29 600 (50 800), 22 500 (24 700), 11 200 (29 400)
$[\mathbf{1b}]^{3+}$	16 800 (32 000), 9700 (19 000)
1d	41 400 (28 600), 28 500 (40 700)
$[\mathbf{1d}]^+$	13 500 (12 200)
2a	29 200 (56 600)
$[\mathbf{2a}]^{+b}$	30 400, 21 600, 10 300, 8400sh
$[\mathbf{2a}]^{2+}$	29 800 (44 700), 22 000 (8500)
$[\mathbf{2a}]^{3+}$	23 900 (22 700), 8700 (22 200)
2d	29 600 (43 200)
$[\mathbf{2d}]^+$	23 400 (23 600), 10 400 (19 100), 8100 (12 400)
$[\mathbf{2d}]^{2+}$	38 600 (28 300), 13 900 (44 800)

^aDetectable by an unresolved weak NIR absorption between 10 000 and 4000 cm^{-1} (see Supporting Information, Figure S6). ^bMolar absorptivity not reported.

The diethynyl–TPA complex **1a** exhibits a pronounced 290 broad absorption band at $\sim 2.8 \times 10^4 \text{ cm}^{-1}$, most likely 291 stemming from the $\pi \rightarrow \pi^*$ intraligand transition with some 292 metal-to-ligand charge transfer contribution, in line with the 293 reported similar systems.^{26–28} The smooth oxidation of neutral 294 **1a** to $[\mathbf{1a}]^+$ conformers leads to the appearance of new intense 295 visible and NIR absorptions and strongly diminished parent UV 296 absorption (Figure 4, top). The asymmetric NIR absorption of 297 $[\mathbf{1a}]^+$ corresponds to an overlap of two sub-bands obtained by 298 deconvolution of the Gaussian function (Supporting Informa- 299 tion, Figure S9 and Table S2). On further oxidation to 300 dicationic species $[\mathbf{1a}]^{2+}$, the characteristic NIR absorption of 301 $[\mathbf{1a}]^+$ gradually disappeared (Figure 4, bottom). The final, well- 302 separated anodic step producing $[\mathbf{1a}]^{3+}$ led to appearance of a 303 new NIR absorption band below $1 \times 10^4 \text{ cm}^{-1}$ (Figure S7) 304 resembling the electronic absorption of oxidized reference 305 $[\mathbf{1d}]^+$ at $1.35 \times 10^4 \text{ cm}^{-1}$ (Figure S10) and, therefore, 306 belonging to the TPA radical cation.²⁹ It has to be considered 307

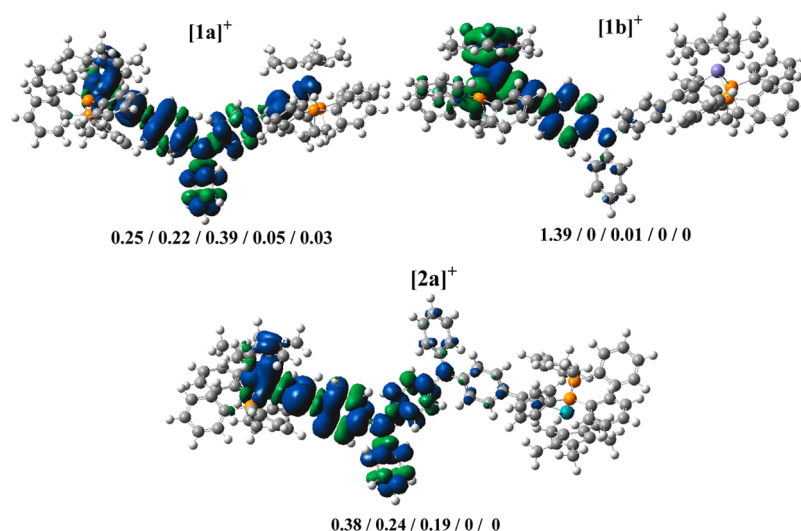


Figure 6. Calculated spin density distribution in $[1a]^+$ and $[2a]^+$ (Ru/C \equiv C/arylamine/C \equiv C/Ru), and $[1b]^+$ (Fe/C \equiv C/arylamine/C \equiv C/Fe). Contour values: ± 0.04 (e/bohr 3) $^{1/2}$. BLYP35/6-31G* (Ru/Fe: Lanl2DZ)/CPCM/CH $_2$ Cl $_2$.

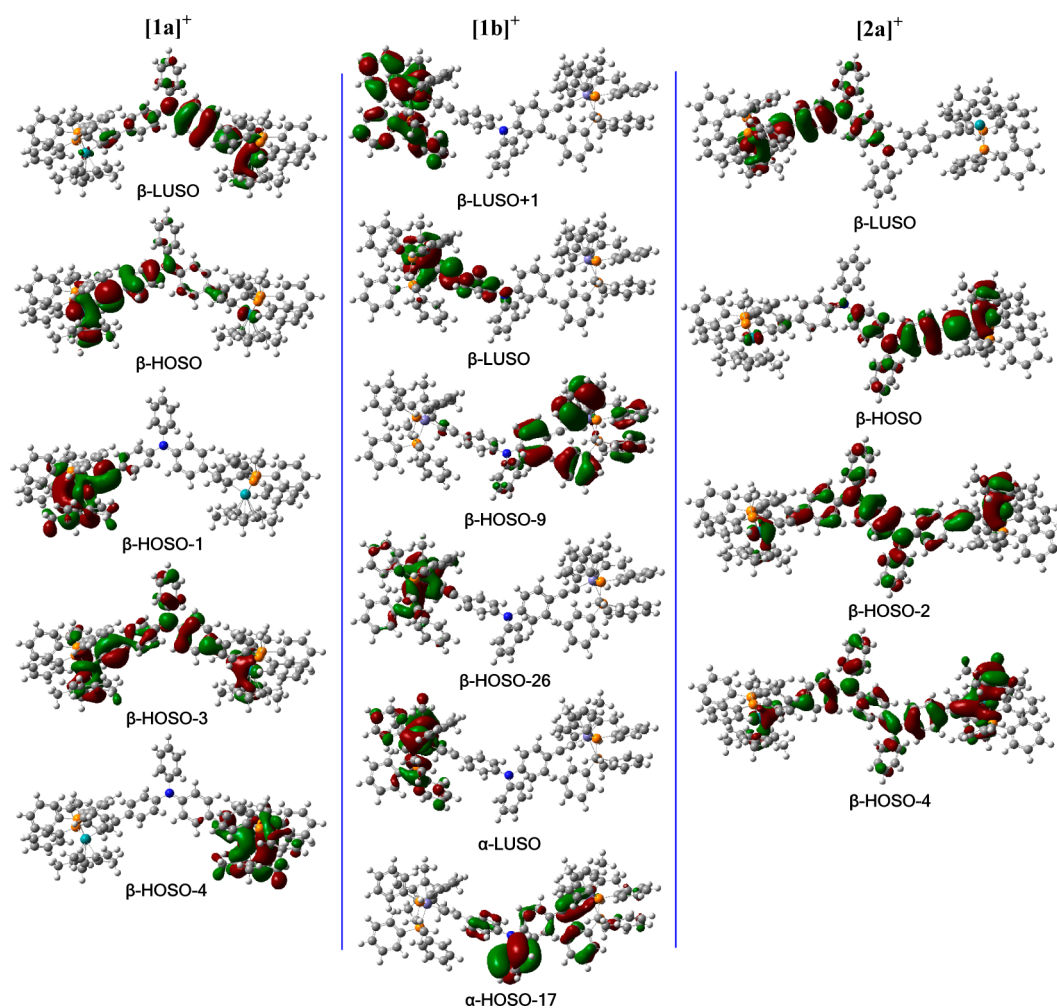


Figure 7. Spin orbitals involved in the major electronic excitations in $[1a]^+$ (left), $[1b]^+$ (middle), and $[2a]^+$ (right) presented in Table 5 (D = doublet). BLYP35/6-31G* (Ru/Fe: Lanl2DZ) /CPCM/CH $_2$ Cl $_2$.

308 that the oxidized Ru–C \equiv C units in precursor $[1a]^{2+}$
 309 somewhat affects the absorption of the cationic bridge-core in
 310 $[1a]^{3+}$, causing its different position and band shape compared
 311 to $[1d]^+$. Thus, the third anodic step of **1a** is mainly localized

on the TPA core, in agreement with the foregoing voltammetric 312
 and IR spectro-electrochemical results. 313

The stepwise oxidation of **1b** to $[1b]^{2+}$ was accompanied by 314
 the instantaneous growth of an intense symmetric absorption 315

Table 5. Major Electronic Excitations in [1a]⁺, [1b]⁺, and [2a]⁺ Determined by the TD-DFT Method^a

complex	excited state	λ (nm) [$\bar{\nu}$ (cm ⁻¹)]	osc strength (<i>f</i>)	major contributions	assignment	$\bar{\nu}$ (cm ⁻¹) (experiment)
[1a] ⁺	D ₂	1306 [7655]	0.43	β -HOSO→ β -LUSO (77%) β -HOSO-4→ β -LUSO (23%)	Ru(1)-C≡C(Ph)→Ru(2)-C≡C(Ph) ⁺ IVCT/ ILET Ru(2) (dppe)Cp*→Ru(2)-C≡C(Ph) ⁺ CT	7900
	D ₄	807 [12 390]	0.10	β -HOSO-1→ β -LUSO (60%) β -HOSO-3→ β -LUSO (33%)	Cp*Ru(1)-C≡C→Ru(2)-C≡C(Ph) ⁺ CT Ru(1)-C≡C-TPA→ Ru(2)-C≡C(Ph) ⁺ CT	10 400
[1b] ⁺	D ₄	1051 [9515]	0.13	β -HOSO-26→ β -LUSO (49%) β -HOSO-9→ β -LUSO (38%)	Cp*(at Fe(2)) ⁺ →Fe(2)-C≡C(Ph) ⁺ ILET Cp*(dppe)C≡C→Fe(2)C≡C(Ph) ⁺ CT	<10 000 (unresolved $\bar{\nu}_{\text{max}}$)
	D ₁₀	568 [17 605]	0.029	β -HOSO-26→ β -LUSO+1 (32%) α -HOSO-17→ α -LUSO (32%)	Cp*(at Fe(2)) ⁺ →dppe(at Fe(2)) ⁺ TPA(C≡C)→FeCp*(dppe) ⁺	not observed
	[2a] ⁺	D ₃	1091 [9165]	0.14	β -HOSO-2→ β -LUSO (75%) β -HOSO→ β -LUSO (25%)	Ru(1)-C≡C-TPPD→Ru(2)-C≡C(Ph) ⁺ ILET/IVCT Ru(1)-C≡C(Ph)→Ru(2)-C≡C(Ph) ⁺ IVCT/ ILET
D ₆		661 [15 130]	0.061	β -HOSO-4→ β -LUSO (65%) β -HOSO-2→ β -LUSO (15%)	Ru(1)-C≡C-TPPD→Ru(2)-C≡C(Ph) ⁺ ILET/IVCT Ru(1)-C≡C-TPPD→Ru(2)-C≡C(Ph) ⁺ ILET/IVCT	10 300

^aThe DFT method was BLYP35/6-31G* (Ru/Fe: LanL2DZ) /CPCM/CH₂Cl₂, D = doublet.

band at 1.12×10^4 cm⁻¹ (Figure 5), reflecting the redox disproportionation of [1b]⁺ to the stable dication and parent **1b**, in agreement with the IR monitoring of the initial anodic process (see above). The low-energy absorption of [1b]²⁺ is reminiscent of ligand-to-metal charge transfer transitions in formally Fe(III) complexes [$\{\text{Fe}(\text{dppe})\text{Cp}^*(\text{C}\equiv\text{C}-)\}_n(\text{Ph})\}^{n+}$ ($n = 1, 2$).³⁰ The striking difference in the NIR electronic absorption between [1b]²⁺ and [1a]²⁺, combined with the poorly separated anodic waves in the former case, does not support participation of the TPA bridge core in the initial oxidation of **1b**. The latter process occurs probably during the subsequent well-separated oxidation of [1b]²⁺ to [1b]³⁺ (Figure S8), as indicated by the comparison with the similar electronic absorption of reference [1d]⁺ (Figure S10) as well as the invariant IR $\nu(\text{C}\equiv\text{C})$ band during this anodic step (Figure 3, right). The product of the initial one-electron oxidation step, [1b]⁺, is hardly observable during the UV-vis-NIR spectroelectrochemical monitoring of the anodic conversion of **1b** to [1b]²⁺ due to the aforementioned redox disproportionation process. However, the weak NIR absorption below 1.1×10^4 cm⁻¹, attributed to unstable [1b]⁺, is clearly seen in the course of the chemical oxidation of **1b** with 1 equiv of FcPF₆ (Supporting Information, Figure S6); its assignment, different from an intervalence charge transfer (IVCT), is presented in the following theoretical (time-dependent (TD) DFT) section.

The observed characteristic UV-vis-NIR spectral changes resulting from the stepwise oxidation of TMS-terminated reference compound **2d** to the corresponding mono- and dication (Supporting Information, Figure S11) are fully consistent with the spectral evolution reported in the literature³¹ for bare TPPD lacking the ethynyl linkers. By contrast, the partly resolved first and second anodic steps of diruthenium diethynyl-TPPD complex **2a** gave rise to UV-vis-NIR absorption changes (Supporting Information, Figure S12) strongly resembling the generation of monocationic diethynyl-TPA-bridged species [1a]⁺, which also matched

their similar IR $\nu(\text{C}\equiv\text{C})$ shifts described in the preceding text. Stable [2a]³⁺ is then characterized by a new UV-vis-NIR absorption (Figure S12, bottom) assigned to the oxidized radical-cationic TPPD core in [2a]³⁺, which is evident from the comparison with the low-lying electronic absorption of reference [2d]⁺ (Figure S11) as well as the negligible change in the $\nu(\text{C}\equiv\text{C})$ wavenumber on oxidation of [2a]²⁺ (Figure S3).

Theoretical Calculations. DFT calculations, using the BLYP35 functional, were performed to gain insight into the electronic structures of the one-electron-oxidized open-shell species [1a]⁺, [1b]⁺, and [2a]⁺, although the latter two cations were not generated in the pure forms during the spectroelectrochemical experiments due to valence disproportionation equilibria resulting in their mixture with the corresponding dications. This applies especially for [1b]⁺ detected only in a very small amount (Supporting Information, Figure S6). The basis set employed here is 6-31G* (LanL2DZ for Ru and Fe atoms). The BLYP35 method reported by Kaupp and coworkers is appropriate for triarylamine and organometallic complexes similar to our systems.^{25,32} All the calculations were performed on nontruncated complexes [1a]⁺, [1b]⁺, and [2a]⁺ to warrant their accuracy, regardless of the relatively heavy computing burden. To account also for solvent effects, the conductor polarizable continuum model (CPCM) in CH₂Cl₂ was employed for the ground-state structural optimization and analyses as well as in TD-DFT calculations of the electronic excitation energies. The pertinent data are presented in Figures 6 and 7, Supporting Information, Figures S13 and S14, and Table 5.

The DFT results indicate similar geometric changes taking place upon the one-electron oxidation of diruthenium complexes **1a** and **2a** (see Supporting Information, Figure S14). The anodic electron transfer results in dominant elongation of one of the C≡C bonds and shorter adjacent (ethynyl)C-Ru, (ethynyl)C-C(phenylene), and N-C-

(phenylene) bonds. The differences between the neutral and monocationic states are greater for **1a**. The diethynyl-TPA bridge is more involved in the initial oxidation of **1a** than the diethynyl-TPPD bridge in **2a**, in agreement with the larger separation of the first two anodic waves for **1a** (Figure 2 and Table 2) reflecting a stronger electronic interaction between the Ru centers mediated by the diethynyl-TPA bridge. In contrast, no significant changes in the bonding characteristics of the diethynyl-TPA bridge accompanied the model oxidation of **1b** that is localized exclusively on the metallic termini. The iron-Cp* centers oxidize independently, and the mixed-valence species, $[\mathbf{1b}]^+$, is unstable with respect to redox disproportionation and conversion to $[\mathbf{1b}]^{2+}$, as was revealed by the UV-vis-NIR spectroscopic monitoring of the anodic path. However, the experimental IR spectro-electrochemical results (Table 3) illustrate that the ethynyl linkers are still involved in the initial oxidation of **1b**, although much less than encountered in both diruthenium complexes, **1a** and **2a**.

The important complementary results obtained with DFT for the spin density distribution in $[\mathbf{1a}]^+$, $[\mathbf{1b}]^+$, and $[\mathbf{2a}]^+$ are shown in Figure 6. Apparently, the spin localization in $[\mathbf{1a}]^+$ and, increasingly, in $[\mathbf{2a}]^+$ and $[\mathbf{1b}]^+$ is asymmetric, residing largely on the ruthenium-ethynyl(-phenylene) and iron-Cp* redox centers, respectively, in one-half of the molecule, which is fully consistent with the symmetry-broken triple bond stretching induced by the initial oxidation of **1a**, **2a**, and **1b** (vide supra). Not surprisingly, the asymmetric spin of $[\mathbf{1a}]^+$ exhibits a delocalized distribution in contrast to the strongly localized oxidation of **1b**, again affirming the effect of the different metal centers on the anodic behavior.

Also worth mentioning is the difference in the spin distribution calculated for radical cations $[\mathbf{1a}]^+$ and $[\mathbf{2a}]^+$ featuring the different bridge cores (Figure 6). In contrast to the delocalized asymmetric spin distribution in $[\mathbf{1a}]^+$, the spin density in $[\mathbf{2a}]^+$ is localized more on one of the Ru centers and less on the bridge core, with no apparent involvement of the remote ruthenium-ethynyl unit, thereby matching well the weak electronic coupling between the ruthenium centers across the elongated TPPD bridge core in $[\mathbf{2a}]^+$ illustrated by the experimental results.

TD-DFT calculations were performed to reproduce the low-energy absorption features in the experimental UV-vis-NIR spectra of the monocationic diethynyl monoamine and diamine complexes and to facilitate their assignment in support of the spin-localized bonding situation (Figure 6). The relevant electronic transitions are presented in Table 5 and depicted in Figure 7. According to the TD-DFT results, the NIR band of $[\mathbf{1a}]^+$ at 7800 cm^{-1} (ν_2 in Figure S9 and Table S2, Supporting Information) has been well-duplicated and can mainly be attributed to the β -HOSO $\rightarrow\beta$ -LUSO transition (HOSO = highest occupied system orbital; LUSO = lowest unoccupied system orbital). The β -HOSO is primarily localized on the nonoxidized Ru-C \equiv C unit (70%), imparting the corresponding transition an appreciable IVCT character. The electronic coupling parameter, $H_{ab} = 685\text{ cm}^{-1}$, was determined from the Hush formula, $H_{ab} = (2.06 \times 10^{-2}/R_{ab})(\epsilon_{\max}\nu_{\max}\Delta\nu)^{1/2}$ (ref 33), in which R_{ab} is the distance between the ruthenium centers in the X-ray crystal structure (Figure 1). Hence, $[\mathbf{1a}]^+$ can be classified as a moderately coupled Robin-Day Class II mixed-valence compound. The higher-lying electronic transition computed at $12\,390\text{ cm}^{-1}$ is most likely responsible for the absorption band of $[\mathbf{1a}]^+$ at $10\,200\text{ cm}^{-1}$ (ν_1 in Figure S9 and Table S2, Supporting Information). It involves both β -HOSO-1

and β -HOSO-3 so that the associated charge transfer to the oxidized Ru(2)-C \equiv C(Ph)⁺ site of $[\mathbf{1a}]^+$ also involves the Cp*(Ru) and TPA donor sites.

Complex $[\mathbf{1b}]^+$ exhibits an NIR excitation at 9515 cm^{-1} belonging to β -HOSO-26 $\rightarrow\beta$ -LUSO and β -HOSO-9 $\rightarrow\beta$ -LUSO transitions. The dominant former component is localized at the oxidized metallic site, having a partial inter-configurational (IC) character typically observed for similar predominantly Fe(III) systems.^{24,34} The acceptor ethynyl(-phenylene) and donor Cp* frameworks are also involved. The second component represents a charge transfer from a ligand-based π -orbital delocalized in the nonoxidized half of $[\mathbf{1b}]^+$. A convincing experimental evidence for this low-energy electronic absorption in valence-localized $[\mathbf{1b}]^+$ with weakly interacting Fe centers is shown in Figure S6 (Supporting Information). The calculated visible electronic absorption of $[\mathbf{1b}]^+$ could not be verified experimentally (Figure 5 and Supporting Information, Figure S6) due to the redox disproportionation of the cation and the tailing absorption of $[\mathbf{1b}]^{2+}$ in that region.

The asymmetric NIR absorptions of $[\mathbf{2a}]^+$ at ca. 8400 and $10\,300\text{ cm}^{-1}$ have been reproduced less accurately than in the case of $[\mathbf{1a}]^+$, probably due to the exaggerated planar conformation of TPPD seen in the computed model. The calculated excitations encompass the dominant β -HOSO-2 $\rightarrow\beta$ -LUSO and β -HOSO-4 $\rightarrow\beta$ -LUSO transitions, respectively. Both β -HOSO-2 and β -HOSO-4 are delocalized over the planar TPPD core and the nonoxidized Ru-C \equiv C unit. Similar to $[\mathbf{1a}]^+$, the β -LUSO resides on the oxidized Ru(2)-C \equiv C(Ph)⁺ site. The IVCT character of the lowest NIR absorption of $[\mathbf{2a}]^+$ becomes enhanced by the 25% admixture of the β -HOSO $\rightarrow\beta$ -LUSO component.

CONCLUSIONS

The electrochemical results reveal that homo-bimetallic complexes **1a**, **1b**, and **2a** undergo multistep oxidation processes. The monocationic state of **1a** is stable, with a large K_c value compared to $[\mathbf{1b}]^+$ that tends to disproportionate to the corresponding dication. Likewise, instability was also expected for $[\mathbf{2a}]^+$ with the extended diamine bridge core, based on the similar poorly resolved first two anodic responses of **1b** and **2a**. However, $[\mathbf{2a}]^+$ could still readily be detected with in situ UV-vis-NIR spectroscopy, bearing a strong resemblance to $[\mathbf{1a}]^+$. Combined results of IR and UV/vis/NIR spectro-electrochemistry and DFT/TD-DFT calculations of nontruncated models have demonstrated that (i) there exists an appreciable electronic interaction between the two ruthenium centers in $[\mathbf{1a}]^+$; (ii) the first two oxidation steps of **1b** are largely Fe-localized; (iii) the spectroscopic characteristics of $[\mathbf{2a}]^+$ indicate much weaker electronic interaction between two ruthenium centers through the extended TPPD bridge core; (iv) the subsequent oxidation of the dications of **1a**, **1b**, and **2a** is localized on the arylamine bridge core (as revealed by IR spectro-electrochemistry and the comparison with the anodic behavior of the corresponding TMS-terminated derivatives). The elongated TPPD linker, with more twisted conformation and restricted π -conjugation, indeed, exhibits electronic insulation properties to some extent. Notably, a planar conformation of TPPD in $[\mathbf{2a}]^+$ and its stronger involvement in the initial oxidation than inferred from the experimental data have emerged from DFT calculations of the model complex. The alternative linear π -conjugated oligoarylamine structures will be the subject of our following report on long-range electron transfer systems. Furthermore, this work may be

513 expedient for designing and investigating more diversified
514 systems with multiple redox states.

515 ■ EXPERIMENTAL SECTION

516 **General Materials.** All manipulations were performed under a dry
517 argon gas atmosphere by using standard Schlenk techniques, unless
518 stated otherwise. Solvents were predried and distilled under argon
519 prior to use, except those used directly for spectroscopic measure-
520 ments, which were of spectroscopic grade. The starting materials 4-
521 bromo-*N*-(4-bromophenyl)-*N*-phenylaniline (**1c**),³⁵ *N*¹,*N*⁴-bis(4-bro-
522 mophenyl)-*N*¹,*N*⁴-diphenylbenzene-1,4-diamine (**2c**),³⁶ [RuCl(dppe)-
523 Cp*],³⁷ and [FeCl(dppe)Cp*]³⁸ were prepared by the procedures
524 described in the literature. Target complexes **1a–1b** and **2a** were
525 prepared along the synthetic route presented in Scheme 1. Other
526 reagents were purchased and used as received.

527 **Syntheses. Intermediate 1d.** To a stirred solution of precursor **1c**
528 (806 mg, 2 mmol), CuI (38 mg, 0.2 mmol), and [Pd(PPh₃)₄] (231
529 mg, 0.2 mmol) in triethylamine (20 mL) and tetrahydrofuran (THF;
530 30 mL) under an argon atmosphere trimethylsilylacetylene (588 mg, 6
531 mmol) was added, and the mixture was held at 60 °C for 24 h. After it
532 cooled, the solution was filtered through a bed of diatomaceous earth.
533 The filtrate was evaporated under reduced pressure and purified by
534 silica gel column chromatography (petroleum ether) to give a light
535 yellow solid (753 mg, yield 86%). ¹H NMR (400 MHz, CDCl₃): δ
536 0.25 (s, 18H, SiMe₃), 6.96 (d, *J*_{HH} = 8 Hz, 4H, Ar–H), 7.06–7.11 (m,
537 4H, Ar–H), 7.32–7.34 (d, *J*_{HH} = 8 Hz, 5H, Ar–H). ¹³C NMR (100
538 MHz, CDCl₃): δ 0.03 (SiMe₃), 93.5, 105.1 (C≡C), 116.9, 123.1,
539 124.1, 124.9, 125.3, 129.3, 129.5, 133.0, 146.5, 147.3 (Ar), as reported
540 in ref 39.

541 **Intermediate 2d.** Compound **2d** was prepared from precursor **2c**
542 by a method analogous to that employed for **1d** and purified on a silica
543 gel column (petroleum ether/dichloromethane = 10:1, v/v) to obtain
544 a light yellow solid (980 mg, yield 81%). ¹H NMR (400 MHz,
545 CDCl₃): δ 0.24 (s, 18H, SiMe₃), 6.98–7.10 (m, 14H, Ar–H), 7.28–
546 7.31 (m, 8H, Ar–H). ¹³C NMR (100 MHz, CDCl₃): δ 0.28 (SiMe₃),
547 93.0, 105.3 (C≡C), 115.8, 121.8, 123.4, 124.7, 125.6, 129.3, 132.8,
548 142.4, 146.8, 147.7 (Ar). EI-MS: *m/z* = 604.55 [M]⁺. Anal. Calcd for
549 C₄₀H₄₀N₂Si₂: C, 79.42; H, 6.66; N, 4.63. Found: C, 79.63; H, 6.58; N,
550 4.67%.

551 **Homo-Bimetallic Complexes 1a, 1b, and 2a.** Target compounds
552 **1a**, **1b**, and **2a** were prepared along the synthetic route presented in
553 Scheme 1.

554 **[[Ru(dppe)Cp*(C≡C)]₂(μ-TPA)] (1a).** A solution of [RuCl(dppe)-
555 Cp*] (321 mg, 0.50 mmol), **1d** (100 mg, 0.23 mmol), and KF (160
556 mg, 2.76 mmol) in CH₃OH (20 mL) and THF (5 mL) was heated to
557 reflux under nitrogen atmosphere for 24 h. The crude product was
558 collected by filtration and washed with hexane. The solid was dissolved
559 in dichloromethane and precipitated by slow diffusion of hexane. The
560 solid was filtered off and dried to give **1a** as a yellow powder (312 mg,
561 yield 87%). ¹H NMR (400 MHz, CDCl₃): δ 1.56 (s, 30H, CH₃ of
562 C₅Me₅), 2.03–2.08 (m, 4H, CH₂ of dppe), 2.66–2.71 (m, 4H, CH₂ of
563 dppe), 6.65–6.76 (m, 8H, Ar–H), 6.86–6.87 (m, 1H, Ar–H), 6.99 (d,
564 2H, *J* = 8 Hz Ar–H), 7.13–7.35 (m, 34H, Ar–H), 7.79 (br, 8H, Ar–
565 H). ¹³C NMR (100 MHz, CDCl₃): δ 10.1 (CH₃ of C₅Me₅), 29.2–31.6
566 (m, CH₂ of dppe), 92.4 (CH₃ of C₅Me₅), 109.1 (Ru–C≡C), 122.4
567 (Ru–C≡C), 123.9–148.3 (m, Ar). ³¹P NMR (160 MHz, CDCl₃): δ
568 78.97 (s, dppe). IR (KBr/cm⁻¹): ν (C≡C) 2062 (w). Anal. Calcd for
569 C₉₄H₉₁NP₄Ru₂: C, 72.34; H, 5.88; N, 0.90. Found: C, 72.56; H, 5.78;
570 N, 0.91%.

571 **[[Fe(dppe)Cp*(C≡C)]₂(μ-TPA)] (1b).** A solution of **1d** (87 mg, 0.20
572 mmol) and K₂CO₃ (61 mg, 0.44 mmol) in CH₃OH (30 mL) and THF
573 (10 mL) was stirred for 10 h under nitrogen atmosphere at room
574 temperature. Then, [FeCl(dppe)Cp*] (275 mg, 0.44 mmol) and
575 Na[BPh₄] (151 mg, 0.44 mmol) were added. After 16 h of stirring,
576 *t*BuOK (52 mg, 0.44 mmol) was introduced, and the mixture was
577 stirred for another 4 h, after which the solvent was evaporated and the
578 residue was extracted with toluene (4 × 10 mL). After the solvent
579 removal, washing with pentane (3 × 10 mL), and vacuum drying, an
580 orange powder was obtained (182 mg, 0.12 mmol, yield 62%). ¹H

NMR (400 MHz, CDCl₃): δ 1.41 (s, 30H, CH₃ of C₅Me₅), 1.96 (br, 581
4H, CH₂ of dppe), 2.64 (br, 4H, CH₂ of dppe), 6.69 (br, 4H, Ar–H), 582
6.81–6.83 (m, 5H, Ar–H), 7.02 (d, *J* = 8 Hz, 2H, Ar–H), 7.24–7.34 583
(m, 34H, Ar–H), 7.91 (br, 8H, Ar–H). ¹³C NMR (100 MHz, 584
CDCl₃): δ 10.1 (CH₃ of C₅Me₅), 30.1–31.6 (m, CH₂ of dppe), 87.5 585
(CH₃ of C₅Me₅), 121.0 (Fe–C≡C), 122.9–138.7 (m, Ar), 142.9 586
(Fe–C≡C). ³¹P NMR (160 MHz, CDCl₃): δ 95.63 (s, dppe). IR 587
(KBr/cm⁻¹): ν (C≡C) 2051 (w). Anal. Calcd for C₉₄H₉₁NP₄Fe₂: C, 588
76.79; H, 6.24; N, 0.95. Found: C, 76.82; H, 6.22; N, 0.96%. 589

590 **[[Ru(dppe)Cp*(C≡C)]₂(μ-TPPD)] (2a).** Complex **2a** was prepared 590
by an analogous method as **1a**, using the following amounts: 591
[RuCl(dppe)Cp*] (464 mg, 0.69 mmol), **2d** (200 mg, 0.33 mmol), 592
and KF (273 mg, 3.96 mmol) dissolved in CH₃OH (20 mL), THF (5 593
mL). The product was obtained as a light green solid (353 mg, 62% 594
yield). ¹H NMR (400 MHz, CDCl₃): δ 1.56 (s, 30H, CH₃ of C₅Me₅), 595
1.99–2.10 (m, 4H, CH₂ of dppe), 2.65–2.76 (m, 4H, CH₂ of dppe), 596
6.70 (d, 4H, *J* = 8 Hz, Ar–H), 6.79 (d, 4H, *J* = 8 Hz, Ar–H), 6.87– 597
6.92 (m, 6H, Ar–H), 7.03 (d, 4H, *J* = 8 Hz Ar–H), 7.17–7.34 (m, 598
36H, Ar–H), 7.79 (br, 8H, Ar–H). ¹³C NMR (100 MHz, CDCl₃): δ 599
10.0 (CH₃ of C₅Me₅), 29.4–29.7 (m, CH₂ of dppe), 92.5 (CH₃ of 600
C₅Me₅), 122.6 (Ru–C≡C), 122.9 (Ru–C≡C), 127.1–133.8 (m, 601
Ar). ³¹P NMR (160 MHz, CDCl₃): δ 70.86 (s, dppe). IR (KBr/cm⁻¹): 602
ν(C≡C) 2067 (s). Anal. Calcd for C₁₀₆H₁₀₀N₂P₄Ru₂: C, 73.68; H, 603
5.83; N, 1.62. Found: C, 73.59; H, 5.80; N, 1.61%. 604

605 **X-ray Crystallography.** Single crystals of complexes **1a** and **2a** 605
suitable for X-ray analysis were grown by layering a solution in 606
dichloromethane with hexane. Crystals with approximate dimensions 607
of 0.20 × 0.20 × 0.10 mm³ for **1a** and 0.20 × 0.20 × 0.20 mm³ for **2a** 608
were mounted on glass fibers for diffraction experiments. Intensity data 609
were collected on a Nonius Kappa CCD diffractometer with Mo Kα 610
radiation (0.710 73 Å) at room temperature. The crystal structures 611
were determined by a combination of direct methods (SHELXS-97)⁴⁰ 612
and Fourier difference techniques, and refined by full matrix least- 613
squares (SHELXL-97).⁴¹ All non-H atoms were refined anisotropically. 614
The hydrogen atoms were placed in ideal positions and refined 615
as riding atoms. The partial solvent molecules were omitted. Further 616
crystal data and details of the data collection are summarized in Table 617
S1. Selected bond distances and angles are given in Table 1. 618

619 **Physical Measurements.** ¹H, ¹³C, and ³¹P NMR spectra were 619
collected on a Varian Mercury Plus 400 spectrometer (400 MHz). ¹H 620
and ¹³C NMR chemical shifts are relative to Si(CH₃)₄ and ³¹P NMR 621
chemical shifts are relative to 85% H₃PO₄. Elemental analyses (C, H, 622
N) were performed with a Vario ElIII Chns instrument. The 623
electrochemical measurements were performed on a CHI 660C 624
potentiostat. A three-electrode single-compartment cell was used for 625
the solution of complexes and supporting electrolyte in dry CH₂Cl₂. 626
The solution was deaerated by argon bubbling on a frit for ~10 min 627
before the measurement. The analyte (complex, ligand) and 628
electrolyte (*n*-Bu₄NPF₆) concentrations were typically 1 × 10⁻³ and 629
1 × 10⁻¹ mol dm⁻³, respectively. A prepolished 500 μm diameter 630
platinum disk working electrode, a platinum wire counter electrode, 631
and an Ag wire pseudoreference electrode were used. Ferrocene was 632
used as the internal potential reference. Spectro-electrochemical 633
experiments at room temperature were performed with an airtight 634
optically transparent thin-layer electrochemical (OTTLE) cell (optical 635
path length of ca. 200 μm) equipped with a Pt minigrid working 636
electrode and CaF₂ windows.⁴² The cell was positioned in the sample 637
compartment of a Bruker Tensor Fourier transform IR spectrometer 638
(1 cm⁻¹ spectral resolution, eight scans) or a Shimadzu UV-3600 UV- 639
vis-NIR spectro-photometer. The controlled-potential electrolyses 640
were performed with a CHI 660C potentiostat. The concentration of 641
analyte samples was ca. 2 × 10⁻³ mol dm⁻³. Dry 3 × 10⁻¹ M *n*- 642
Bu₄NPF₆ was used as the supporting electrolyte. 643

644 **Computational Details.** DFT calculations were performed with 644
the Gaussian 09 program,⁴³ at the BLYP35⁴⁴/6-31G* level of theory. 645
The basis set employed was 6-31G* (Lanl2DZ for Ru and Fe atoms). 646
Geometry optimization was performed without any symmetry 647
constraints. Electronic transitions were calculated by the TD-DFT 648
method. The molecular orbital contributions were generated using the 649
Multiwfn package and plotted using GaussView 5.0. The solvation 650

651 effects in dichloromethane are included for a part of the calculations
652 with the CPCM.⁴⁵

653 ■ ASSOCIATED CONTENT

654 ● Supporting Information

655 The Supporting Information is available free of charge on the
656 ACS Publications website at DOI: 10.1021/acs.inorg-
657 chem.6b02809.

658 Crystallographic information, additional spectro-electro-
659 chemical information, additional calculated DFT data,
660 ¹H, ¹³C and ³¹P NMR spectra of the new compounds.
661 (PDF)

662 Crystallographic data (CIF)

663 Crystallographic data (CIF)

664 ■ AUTHOR INFORMATION

665 Corresponding Authors

666 *E-mail: f.hartl@reading.ac.uk. (F.H.)

667 *E-mail: chshliu@mail.ccnu.edu.cn. (S.H.L.)

668 ORCID

669 František Hartl: 0000-0002-7013-5360

670 Notes

671 The authors declare no competing financial interest.

672 ORCID, Frantisek Hartl: 0000-0002-7013-5360

673 ■ ACKNOWLEDGMENTS

674 The authors acknowledge financial support from National
675 Natural Science Foundation of China (21272088, 21472059,
676 21402057), the self-determined research funds of the CCNU
677 from the colleges' basic research and operation of MOE
678 (CCNU14A05009, CCNU14F01003), and the Excellent
679 Doctoral Dissertation Cultivation Grant from the Central
680 China Normal University (2015YBYB108, 2016YBZZ040).

681 ■ REFERENCES

682 (1) (a) Ren, T. Diruthenium σ -alkynyl compounds: a new class of
683 conjugated organometallics. *Organometallics* **2005**, *24*, 4854–4870.
684 (b) Qi, H.; Noll, B.; Snider, G. L.; Lu, Y.; Lent, S. S.; Fehlner, T. P.;
685 Gupta, A. Dependence of field switched ordered arrays of dinuclear
686 mixed-valence complexes on the distance between the redox centers
687 and the size of the counterions. *J. Am. Chem. Soc.* **2005**, *127*, 15218–
688 15227. (c) Schwab, P. F. H.; Smith, J. R.; Michl, J. Synthesis and
689 properties of molecular rods. 2. Zig-zag rods. *Chem. Rev.* **2005**, *105*,
690 1197–1279. (d) Burgun, A.; Ellis, B. G.; Roisnel, T.; Skelton, B. W.;
691 Bruce, M. I.; Lapinte, C. From molecular wires to molecular resistors:
692 TCNE, a class-III/class-II mixed-valence chemical switch. *Organo-*
693 *metallics* **2014**, *33*, 4209–4219. (e) Blum, A. S.; Ren, T.; Parish, D. A.;
694 Trammell, S. A.; Moore, M. H.; Kushmerick, J. G.; Xu, G. L.;
695 Deschamps, J. R.; Pollack, S. K.; Shashidhar, R. Ru₂(ap)₄ (σ -
696 oligo(phenyleneethynyl)) molecular wires: synthesis and electronic
697 characterization. *J. Am. Chem. Soc.* **2005**, *127*, 10010–10011.
698 (2) (a) Crutchley, R. J. Intervalence charge transfer and electron
699 exchange studies of dinuclear ruthenium complexes. *Adv. Inorg. Chem.*
700 **1994**, *41*, 273–325. (b) Schwab, P. F. H.; Levin, M. D.; Michl, J.
701 Molecular rods. I. Simple axial rods. *Chem. Rev.* **1999**, *99*, 1863–1933.
702 (c) Xu, G. L.; Crutchley, R. J.; DeRosa, M. C.; Pan, Q. J.; Zhang, H. X.;
703 Wang, X.; Ren, T. Strong electronic couplings between ferrocenyl
704 centers mediated by bis-ethynyl/butadiynyl diruthenium bridges. *J.*
705 *Am. Chem. Soc.* **2005**, *127*, 13354–13365. (d) Zhu, X. X.; Ou, Y. P.;
706 Zhang, J.; Xia, J. L.; Yin, J.; Yu, G.-A.; Liu, S. H. Dithia[3.3]-
707 paracyclophane-based monometal ruthenium acetylide complexes:
708 synthesis, characterization and substituent effects. *Dalton Trans.*
709 **2013**, *42*, 7177–7189. (e) Xia, J. L.; Man, W. Y.; Zhu, X.; Zhang,
710 C.; Jin, G.; Schauer, P. A.; Fox, M. A.; Yin, J.; Yu, G.; Low, P. J.; Liu, S.

H. Synthesis and characterization of dithia[3.3]paracyclophane-
711 bridged binuclear ruthenium vinyl and alkynyl complexes. *Organo-*
712 *metallics* **2012**, *31*, 5321–5333. (f) Man, W. Y.; Xia, J. L.; Brown, N. J.;
713 Farmer, J. D.; Yufit, D. S.; Howard, J. A. K.; Liu, S. H.; Low, P. J.
714 Spectroscopic and computational studies of the ligand redox non-
715 innocence in mono- and binuclear ruthenium vinyl complexes. *716*
Organometallics **2011**, *30*, 1852–1858. (g) Ou, Y. P.; Zhang, J.; Xu,
717 M.; Xia, J. L.; Hartl, F.; Yin, J.; Yu, G. A.; Liu, S. H. Bridge-localized
718 HOMO-binding character of divinylanthracene-bridged dinuclear
719 ruthenium carbonyl complexes: spectroscopic, spectroelectrochemical,
720 and computational studies. *Chem. - Asian J.* **2014**, *9*, 1152–1160.
721 (h) Ou, Y. P.; Zhang, J.; Zhang, F.; Kuang, D.; Hartl, F.; Rao, L.; Liu,
722 S. H. Notable differences between oxidized diruthenium complexes
723 bridged by four isomeric diethynyl benzodithiophene ligands. *Dalton*
724 *Trans.* **2016**, *45*, 6503–6516. (i) Ou, Y. P.; Xia, J. L.; Zhang, J.; Xu, M.;
725 Yin, J.; Yu, G. A.; Liu, S. H. Experimental and theoretical studies of
726 charge delocalization in biruthenium-alkynyl complexes bridged by
727 thiophenes. *Chem. - Asian J.* **2013**, *8*, 2023–2032. 728

(3) (a) Kaim, W. Concepts for metal complex chromophores
729 absorbing in the near infrared. *Coord. Chem. Rev.* **2011**, *255*, 2503–
730 2513. (b) Costuas, K.; Rigaut, S. Polynuclear carbon-rich organo-
731 metallic complexes: clarification of the role of the bridging ligand in
732 the redox properties. *Dalton Trans.* **2011**, *40*, 5643–5658. (c) Halet, J.-
733 F.; Lapinte, C. Charge delocalization vs localization in carbon-rich iron
734 mixed-valence complexes: A subtle interplay between the carbon
735 spacer and the (dppe)Cp*Fe organometallic electrophore. *Coord.*
736 *Chem. Rev.* **2013**, *257*, 1584–1613. (d) Cao, Z.; Xi, B.; Jodoin, D. S.;
737 Zhang, L.; Cummings, S. P.; Gao, Y.; Tyler, S. F.; Fanwick, P. E.;
738 Crutchley, R. J.; Ren, T. Diruthenium-polyyn-diyl-diruthenium
739 wires: electronic coupling in the long distance regime. *J. Am. Chem.*
740 *Soc.* **2014**, *136*, 12174–12183. (e) Brunschwig, B. S.; Creutz, C.; Sutin,
741 N. Electroabsorption spectroscopy of charge transfer states of
742 transition metal complexes. *Coord. Chem. Rev.* **1998**, *177*, 61–79.
743 (f) Scheerer, S.; Rothowe, N.; Abdel-Rahman, O. S.; He, X.; Rigaut,
744 S.; Kvapilová, H.; Winter, R. F.; et al. Vinyl ruthenium-modified
745 biphenyl and 2, 2'-bipyridines. *Inorg. Chem.* **2015**, *54*, 3387–3402.
746 (g) Launay, J.-P. Long-distance intervalence electron transfer. *Chem.*
747 *Soc. Rev.* **2001**, *30*, 386–397. 748

(4) (a) Carroll, R. L.; Gorman, C. B. The genesis of molecular
749 electronics. *Angew. Chem., Int. Ed.* **2002**, *41*, 4378–4400. (b) Bennis-
750 ton, A. C. Pushing around electrons: towards 2-D and 3-D molecular
751 switches. *Chem. Soc. Rev.* **2004**, *33*, 573–578. (c) Gluyas, J. B. G.;
752 Boden, A. J.; Eaves, S. G.; Yu, H.; Low, P. J. Cross-conjugated systems
753 based on an (E)-hexa-3-en-1,5-diyne-3,4-diyl skeleton: spectroscopic
754 and spectroelectrochemical investigations. *Dalton Trans.* **2014**, *43*,
755 6291–6294. (d) Paul, F.; Lapinte, C. Organometallic molecular wires
756 and other nanoscale-sized devices: an approach using the organoiron
757 (dppe)Cp*Fe building block. *Coord. Chem. Rev.* **1998**, *178–180*, 431–
758 509. (e) Martin, R. E.; Diederich, F. Lineare monodisperse π -
759 konjugierte oligomere: mehr als nur modellverbindungen für
760 polymere. *Angew. Chem.* **1999**, *111*, 1440–1469. (f) Martin, R. E.;
761 Diederich, F. Linear monodisperse π -conjugated oligomers: model
762 compounds for polymers and more. *Angew. Chem., Int. Ed.* **1999**, *38*,
763 1350–1377. (g) Yao, C.-J.; Zhong, Y.-W.; Yao, J. N. Charge
764 delocalization in a cyclometalated bisruthenium complex bridged by
765 a noninnocent 1,2,4,5-tetra(2-pyridyl)benzene ligand. *J. Am. Chem.*
766 *Soc.* **2011**, *133*, 15697–15706. (h) Maurer, J.; Sarkar, B.; Schwederski,
767 B.; Kaim, W.; Winter, R. F.; Zális, S. Divinylphenylene-bridged
768 diruthenium complexes bearing Ru(CO)Cl(PⁱPr)₃ entities. *Organo-*
769 *metallics* **2006**, *25*, 3701–3712. (i) Pevny, F.; Di Piazza, E.; Norel, L.;
770 Drescher, M.; Winter, R. F.; Rigaut, S. Fully delocalized (ethynyl)
771 (vinyl) phenylene-bridged diruthenium radical complexes. *Organo-*
772 *metallics* **2010**, *29*, 5912–5918. 773

(5) (a) Whittall, I. R.; McDonagh, A. M.; Humphrey, M. G.; Marek,
774 S. Organometallic complexes in nonlinear optics II: third-order
775 nonlinearities and optical limiting studies. *Adv. Organomet. Chem.*
776 **1999**, *43*, 349–405. (b) Mayor, M.; von Hänisch, C.; Weber, H. B.;
777 Reichert, J.; Beckmann, D. Ein trans-Platin (II)-Komplex als
778 Einzelmolekülisolator. *Angew. Chem.* **2002**, *114*, 1228–1231. 779

- (c) Mayor, M.; von Hänisch, C.; Weber, H. B.; Reichert, J.; Beckmann, D. A trans-platinum (II) complex as a single-molecule insulator. *Angew. Chem., Int. Ed.* **2002**, *41*, 1183–1186. (d) Schull, T. L.; Kushmerick, J. G.; Patterson, C. H.; George, C.; Moore, M. H.; Pollack, S. K.; Shashidhar, R. Ligand effects on charge transport in platinum (II) acetylides. *J. Am. Chem. Soc.* **2003**, *125*, 3202–3203. (e) Pfaff, U.; Hildebrandt, A.; Korb, M.; Lang, H. The influence of an ethynyl spacer on the electronic properties in 2, 5-ferrocenyl-substituted heterocycles. *Polyhedron* **2015**, *86*, 2–9. (f) Miesel, D.; Hildebrandt, A.; Korb, M.; Wild, D. A.; Low, P. J.; Lang, H. Influence of P-bonded bulky substituents on electronic interactions in ferrocenyl-substituted phospholes. *Chem. - Eur. J.* **2015**, *21*, 11545–11559. (g) Gidron, O.; Diskin-Posner, Y.; Bendikov, M. High charge delocalization and conjugation in oligofuran molecular wires. *Chem. - Eur. J.* **2013**, *19*, 13140–13150.
- (6) (a) Maurer, J.; Linseis, M.; Sarkar, B.; Schwederski, B.; Niemeyer, M.; Kaim, W.; Zálaiš, S.; Anson, C.; Zabel, M.; Winter, R. F. Ruthenium complexes with vinyl, styryl, and vinylpyrenyl ligands: A case of non-innocence in organometallic chemistry. *J. Am. Chem. Soc.* **2008**, *130*, 259–268. (b) Linseis, M.; Zálaiš, S.; Zabel, M.; Winter, R. F. Ruthenium stilbenyl and diruthenium distyrylethene complexes: aspects of electron delocalization and electrocatalyzed isomerization of the Z-isomer. *J. Am. Chem. Soc.* **2012**, *134*, 16671–16692. (c) Zálaiš, S.; Winter, R. F.; Kaim, W. Quantum chemical interpretation of redox properties of ruthenium complexes with vinyl and TCNX type non-innocent ligands. *Coord. Chem. Rev.* **2010**, *254*, 1383–1396. (d) Lloveras, V.; Caballero, A.; Tárraga, A.; Velasco, M. D.; Espinosa, A.; Wurst, K.; Evans, D. J.; Vidal-Gancedo, J.; Rovira, C.; Molina, P.; Veciana, J. Synthesis and characterization of radical cations derived from mono- and biferoenyl-substituted 2-aza-1, 3-butadienes: a study of the influence of an asymmetric and oxidizable bridge on intramolecular electron transfer. *Eur. J. Inorg. Chem.* **2005**, *2005*, 2436–2450.
- (7) (a) Creutz, C.; Taube, H. Direct approach to measuring the Franck-Condon barrier to electron transfer between metal ions. *J. Am. Chem. Soc.* **1969**, *91*, 3988–3989. (b) Creutz, C.; Taube, H. Binuclear complexes of ruthenium ammines. *J. Am. Chem. Soc.* **1973**, *95*, 1086–1094. (c) Demadis, K. D.; Hartshorn, C. M.; Meyer, T. J. The localized-to-delocalized transition in mixed-valence chemistry. *Chem. Rev.* **2001**, *101*, 2655–2686. (d) Nelsen, S. F. "Almost Delocalized" Intervalence Compounds. *Chem. - Eur. J.* **2000**, *6*, 581–588. (e) Yamamoto, M.; Onitsuka, K.; Uno, M.; Takahashi, S. Synthesis of enantiopure planar-chiral cyclopentadienyl-ruthenium binuclear complexes bridged by aromatic systems. *J. Chem. Soc., Dalton Trans.* **2002**, 1473–1478. (f) Onitsuka, K.; Harada, Y.; Takahashi, S. Synthesis and properties of chiral organometallic polymers with (R)-3,3'-diethynyl-1,1'-binaphthyl bridges. *Synth. Met.* **2009**, *159*, 982–985.
- (8) (a) Tanaka, Y.; Shaw-Taberlet, J. A.; Justaud, F.; Cador, O.; Roisnel, T.; Akita, M.; Hamon, J.-R.; Lapinte, C. Electronic and magnetic couplings in free and π -coordinated 1,4-diethynyl-naphthalene-bridged $[\text{Cp}^*(\text{dppe})\text{Fe}]^{n+}$ ($n = 0, 1$) units. *Organometallics* **2009**, *28*, 4656–4669. (b) Low, P. J. Twists and turns: studies of the complexes and properties of bimetallic complexes featuring phenylene ethynylene and related bridging ligands. *Coord. Chem. Rev.* **2013**, *257*, 1507–1532. (c) Gao, L.-B.; Kan, J.; Fan, Y.; Zhang, L.-Y.; Liu, S.-H.; Chen, Z.-N. Wirelike dinuclear ruthenium complexes connected by bis(ethynyl)oligothiophene. *Inorg. Chem.* **2007**, *46*, 5651–5664. (d) Low, P. J. Metal complexes in molecular electronics: progress and possibilities. *Dalton Trans.* **2005**, 2821–2824. (e) Akita, M.; Koike, T. Chemistry of polycarbon species: from clusters to molecular devices. *Dalton Trans.* **2008**, 3523–3530. (f) Ying, J.-W.; Liu, I. P. C.; Xi, B.; Song, Y.; Campana, C.; Zuo, J.-L.; Ren, T. Linear trimer of diruthenium linked by butadien-diyl units: a unique electronic wire. *Angew. Chem., Int. Ed.* **2010**, *49*, 954–957. (g) Fan, Y.; Zhang, L.-Y.; Dai, F.-R.; Shi, L.-X.; Chen, Z.-N. Preparation, characterization, and photophysical properties of Pt-M ($M = \text{Ru}, \text{Re}$) heteronuclear complexes with 1,10-phenanthrolineethynyl ligands. *Inorg. Chem.* **2008**, *47*, 2811–2819.
- (9) (a) Li, D.; Sun, X.; Wang, M.; Yu, H.; Zhou, H.; Wu, J.; Tian, Y. Novel colorimetric detection probe for copper (II) ions based on triphenylamine mixed-valence chromophores bearing prodigious two-photon absorption activity. *Sens. Actuators, B* **2015**, *220*, 1006–1016. (b) Rovira, C.; Ruiz-Molina, D.; Elsner, O.; Vidal-Gancedo, J.; Bonvoisin, J.; Launay, J. P.; Veciana, J. Influence of topology on the long-range electron-transfer phenomenon. *Chem. - Eur. J.* **2001**, *7*, 240–250. (c) Gautier, N.; Dumur, F.; Lloveras, V.; Vidal-Gancedo, J.; Veciana, J.; Rovira, C.; Hudhomme, P. Intramolecular electron transfer mediated by a tetrathiafulvalene bridge in a purely organic mixed-valence system. *Angew. Chem.* **2003**, *115*, 2871–2874. (d) Lindeman, S. V.; Rosokha, S. V.; Sun, D.; Kochi, J. K. X-ray structure analysis and the intervalent electron transfer in organic mixed-valence crystals with bridged aromatic cation radicals. *J. Am. Chem. Soc.* **2002**, *124*, 843–855. (e) Rosokha, S. V.; Sun, D. L.; Kochi, J. K. Conformation, distance, and connectivity effects on intramolecular electron transfer between phenylene-bridged aromatic redox centers. *J. Phys. Chem. A* **2002**, *106*, 2283–2292. (f) Bailey, S. E.; Zink, J. L.; Nelsen, S. F. Contributions of symmetric and asymmetric normal coordinates to the intervalence electronic absorption and resonance raman spectra of a strongly coupled p-phenylenediamine radical cation. *J. Am. Chem. Soc.* **2003**, *125*, 5939–5947.
- (10) (a) Nelsen, S. F.; Konradsson, A. E.; Weaver, M. N.; Telo, J. P. Intervalence near-IR spectra of delocalized dinitroaromatic radical anions. *J. Am. Chem. Soc.* **2003**, *125*, 12493–12501. (b) Mayor, M.; Büschel, M.; Fromm, K. M.; Lehn, J. M.; Daub, J. Electron transfer through molecular bridges between reducible pentakis(thiophenyl) benzene subunits. *Chem. - Eur. J.* **2001**, *7*, 1266–1272. (c) D'Alessandro, D. M.; Topley, A. C.; Davies, M. S.; Keene, F. R. Probing the transition between the localised (Class II) and localized-to-delocalised (Class II-III) regimes by using intervalence charge-transfer solvatochromism in a series of mixed-valence dinuclear ruthenium complexes. *Chem. - Eur. J.* **2006**, *12*, 4873–4884.
- (11) (a) Heckmann, A.; Amthor, S.; Lambert, C. Mulliken-Hush analysis of a bis (triarylamine) mixed-valence system with a N $\bullet\bullet\bullet$ N distance of 28.7 Å. *Chem. Commun.* **2006**, *42*, 2959–2961. (b) Hanss, D.; Walther, M. E.; Wenger, O. S. Importance of covalence, conformational effects and tunneling-barrier heights for long-range electron transfer: insights from dyads with oligo-p-phenylene, oligo-p-xylene and oligo-p-dimethoxybenzene bridges. *Coord. Chem. Rev.* **2010**, *254*, 2584–2592. (c) Banerjee, M.; Shukla, R.; Rathore, R. Synthesis, optical, and electronic properties of soluble poly-p-phenylene oligomers as models for molecular wires. *J. Am. Chem. Soc.* **2009**, *131*, 1780–1786. (d) Garmshausen, Y.; Schwarz, J.; Hildebrandt, J.; Kobin, B.; Pätzelt, M.; Hecht, S. Making nonsymmetrical bricks: synthesis of insoluble dipolar sexiphenyls. *Org. Lett.* **2014**, *16*, 2838–2841. (e) Miyata, Y.; Nishinaga, T.; Komatsu, K. Synthesis and structural, electronic, and optical properties of oligo(thienylfuran)s in comparison with oligothiophenes and oligofurans. *J. Org. Chem.* **2005**, *70*, 1147–1153.
- (12) (a) Polit, W.; Mücke, P.; Wuttke, E.; Exner, T.; Winter, R. F. Charge and spin confinement to the amine site in 3-connected triarylamine vinyl ruthenium conjugates. *Organometallics* **2013**, *32*, 5461–5472. (b) Dapperheld, S.; Steckhan, E.; Brinkhaus, K. H. G.; Esch, T. Organic electron transfer systems, II substituted triarylamine cation-radical redox systems-synthesis, electrochemical and spectroscopic properties, Hammett behavior, and suitability as redox catalysts. *Chem. Ber.* **1991**, *124*, 2557–2567. (c) Bender, T. P.; Graham, J. F.; Duff, J. M. Effect of substitution on the electrochemical and xerographic properties of triarylamine: correlation to the Hammett parameter of the substituent and calculated HOMO energy level. *Chem. Mater.* **2001**, *13*, 4105–4111. (d) Walter, R. I. Substituent effects on the properties of stable aromatic free radicals. The criterion for non-hammett behavior I. *J. Am. Chem. Soc.* **1966**, *88*, 1923–1930. (e) Amthor, S.; Noller, B.; Lambert, C. UV/Vis/NIR spectral properties of triarylamine and their corresponding radical cations. *Chem. Phys.* **2005**, *316*, 141–152.
- (13) (a) Connelly, N. G.; Geiger, W. E. Chemical redox agents for organometallic chemistry. *Chem. Rev.* **1996**, *96*, 877–910. (b) Tang, C.

- 918 W.; VanSlyke, A. S. Organic electroluminescent diodes. *Appl. Phys. Lett.* **1987**, *51*, 913–915. (c) Law, K. Y. Organic photoconductive materials: recent trends and developments. *Chem. Rev.* **1993**, *93*, 449–921 406.
- 922 (14) (a) Haridas, K. R.; Ostrauskaite, J.; Thelakkat, M.; Heim, M.; Bilke, R.; Haarer, D. Synthesis of low melting hole conductor systems based on triarylamine and application in dye sensitized solar cells. *Synth. Met.* **2001**, *121*, 1573–1574. (b) Bacher, E.; Bayerl, M.; Rudati, P.; Reckefuss, N.; Mueller, C. D.; Meerholz, K.; Nuyken, O. Synthesis and characterization of photo-cross-linkable hole-conducting polymers. *Macromolecules* **2005**, *38*, 1640–1647. (c) Kido, J.; Kimura, M.; Nagai, K. Multilayer white light-emitting organic electroluminescent device. *Science* **1995**, *267*, 1332–1334. (d) Gu, G.; Bulović, V.; Burrows, P. E.; Forrest, S. R.; Thompson, M. E. Transparent organic light emitting devices. *Appl. Phys. Lett.* **1996**, *68*, 2606–2608. (e) Cremer, J.; Bauerle, P.; Wienk, M. M.; Janssen, R. A. J. High open-circuit voltage poly(ethynylene bithienylene):fullerene solar cells. *Chem. Mater.* **2006**, *18*, 5832–5834. (f) Moerner, W. E.; Silence, S. M. Polymeric photorefractive materials. *Chem. Rev.* **1994**, *94*, 127–155. (g) Yen, H. J.; Guo, S. M.; Liou, G. S.; Chung, J. C.; Liu, Y. C.; Lu, Y. F.; Zeng, Y. Z. Mixed-valence class I transition and electrochemistry of bis-(triphenylamine)-based aramids containing isolated ether-linkage. *J. Polym. Sci., Part A: Polym. Chem.* **2011**, *49*, 3805–3816.
- 941 (15) (a) Zhou, G.; Baumgarten, M.; Mullen, K. Arylamine-substituted oligo(ladder-type pentaphenylene)s: electronic communication between bridged redox centers. *J. Am. Chem. Soc.* **2007**, *129*, 12211–12221. (b) Lambert, C.; Risko, C.; Coropceanu, V.; Schelter, J.; Amthor, S.; Gruhn, N. E.; Durivage, J. C.; Brédas, J.-L. Electronic coupling in tetraanisylarylenediamine mixed-valence systems: The interplay between bridge energy and geometric factors. *J. Am. Chem. Soc.* **2005**, *127*, 8508–8516. (c) Lancaster, K.; Odom, S. A.; Jones, S. C.; Thayumanavan, S.; Marder, S. R.; Brédas, J.-L.; Coropceanu, V.; Barlow, S. Intramolecular electron-transfer rates in mixed-valence triarylamine: measurement by variable-temperature ESR spectroscopy and comparison with optical data. *J. Am. Chem. Soc.* **2009**, *131*, 1717–1723. (d) Seo, E. T.; Nelson, R. F.; Fritsch, J. M.; Marcoux, L. S.; Leedy, D. W.; Adams, R. N. Anodic oxidation pathways of aromatic amines. Electrochemical and electron paramagnetic resonance studies. *J. Am. Chem. Soc.* **1966**, *88*, 3498–3503.
- 957 (16) (a) Hankache, J.; Wenger, O. S. Organic mixed valence. *Chem. Rev.* **2011**, *111*, 5138–5178. (b) Ramirez, C. L.; Pegoraro, C. N.; Filevich, O.; Bruttomeso, A.; Etchenique, R.; Parise, A. R. Role of ruthenium oxidation states in ligand-to-ligand charge transfer processes. *Inorg. Chem.* **2012**, *51*, 1261–1268. (c) Parthey, M.; Vincent, K. B.; Schauer, M. R. P. A.; Yufit, D. S.; Howard, J. A. K.; Kaupp, M.; Low, P. J.; Renz, M. A Combined computational and spectroelectrochemical study of platinum-bridged bis-triarylamine systems. *Inorg. Chem.* **2014**, *53*, 1544–1554. (d) Lambert, C.; Amthor, S.; Schelter, J. From valence trapped to valence delocalized by bridge state modification in bis(triarylamine) radical cations: evaluation of coupling matrix elements in a three-level system. *J. Phys. Chem. A* **2004**, *108*, 6474–6486. (e) Seibt, J.; Schaumlöffel, A.; Lambert, C.; Engel, V. Quantum study of the absorption spectroscopy of bis(triarylamine) radical cations. *J. Phys. Chem. A* **2008**, *112*, 10178–10184. (f) Heckmann, A.; Lambert, C. Organic mixed-valence compounds: a playground for electrons and holes. *Angew. Chem., Int. Ed.* **2012**, *51*, 326–392.
- 975 (17) (a) Huang, C.-Y.; Hsu, C.-Y.; Yang, L.-Y.; Lee, C.-J.; Yang, T.-F.; Hsu, C.-C.; Ke, C.-H.; Su, Y. O. A systematic study of electrochemical and spectral properties for the electronic interactions in porphyrin–triphenylamine conjugates. *Eur. J. Inorg. Chem.* **2012**, *2012*, 1038–1047. (b) Yao, C.-J.; Zhong, Y.-W.; Yao, J. Five-stage near-infrared electrochromism in electropolymerized films composed of alternating cyclometalated bisruthenium and bis-triarylamine segments. *Inorg. Chem.* **2013**, *52*, 10000–10008. (c) Lambert, C.; Nöll, G.; Schelter, J. Bridge-mediated hopping or superexchange electron-transfer processes in bis(triarylamine) systems. *Nat. Mater.* **2002**, *1*, 69–73. (d) Low, P. J.; Paterson, M. A.; Puschmann, H.; Goeta, A. E.; Howard, J. A.; Lambert, C.; Cherryman, J. C.; Tackley, D. R.; Leeming, S.; Brown, B. Crystal, Molecular and electronic structure of N,N' -diphenyl- N,N' -bis(2,4-dimethylphenyl)-1,1'-biphenyl)-4, 4'-diamine and the corresponding radical cation. *Chem. - Eur. J.* **2004**, *10*, 83–91. (e) Barlow, S.; Risko, C.; Odom, S. A.; Zheng, S.; Coropceanu, V.; Beverina, L.; Brédas, J.-L.; Marder, S. R. Tuning delocalization in the radical cations of 1,4-bis[4-(diarylamine)styryl]benzenes, 2,5-bis[4-(diarylamine)styryl]thiophenes, and 2, 5-bis[4-(diarylamine)styryl]pyrroles through substituent effects. *J. Am. Chem. Soc.* **2012**, *134*, 10146–10155.
- 994 (18) (a) Grelaud, G.; Cador, O.; Roisnel, T.; Argouarch, G.; Cifuentes, M. P.; Humphrey, M. G.; Paul, F. Triphenylamine derivatives with para-disposed pendant electron-rich organoiron alkynyl substituents: defining the magnetic interactions in a trinuclear iron (III) trication. *Organometallics* **2012**, *31*, 1635–1642. (b) Cui, B.; Tang, J.-H.; Yao, J.-N.; Zhong, Y.-W. A molecular platform for multistate near-infrared electrochromism and flip-flop, flip-flap-flop, and ternary memory. *Angew. Chem., Int. Ed.* **2015**, *54*, 9192–9197. (c) Fink, D.; Weibert, B.; Winter, R. F. Redox-active tetraruthenium metallacycles: reversible release of up to eight electrons resulting in strong electrochromism. *Chem. Commun.* **2016**, *52*, 6103–6106. (d) Polit, W.; Exner, T.; Wuttke, E.; Winter, R. F. Vinylruthenium-triarylamine conjugates as electroswitchable polyelectrochromic NIR dyes. *BioInorg. React. Mech.* **2012**, *8*, 85–105. (e) Tang, J.-H.; Shao, J.-Y.; He, Y.-Q.; Wu, S.-H.; Yao, J.; Zhong, Y.-W. Transition from a metal-localized mixed-valence compound to a fully delocalized and bridge-biased electrophore in a ruthenium-amine-ruthenium tricenter system. *Chem. - Eur. J.* **2016**, *22*, 10341. (f) Cheng, H.-C.; Chiu, K. Y.; Lu, S. H.; Chen, C.-C.; Lee, Y. W.; Yang, T.-F.; Kuo, M. Y.; Chen, P. P. Y.; Su, Y. O. Linear oligoarylamines: electrochemical, EPR, and computational studies of their oxidative states. *J. Phys. Chem. A* **2015**, *119*, 1933–1942. (g) Onitsuka, K.; Ohara, N.; Takei, F.; Takahashi, S. Synthesis and redox properties of trinuclear ruthenium–acetylide complexes with tri(ethynylphenyl)amine bridge. *Dalton Trans.* **2006**, 3693–3698. (h) Grelaud, G.; Cifuentes, M. P.; Schwich, T.; Argouarch, G.; Petrie, S.; Stranger, R.; Paul, F.; Humphrey, M. G. Multistate redox-active metalated triarylamine. *Eur. J. Inorg. Chem.* **2012**, *2012*, 65–75. (i) Onitsuka, K.; Ohara, N.; Takei, F.; Takahashi, S. Organoruthenium dendrimers possessing tris(4-ethynylphenyl)-amine bridges. *Organometallics* **2008**, *27*, 25–27.
- 1025 (19) (a) Paul, F.; Lapinte, C. Organometallic molecular wires and other nanoscale-sized devices: an approach using the organoiron-(dppe)Cp*Fe building block. *Coord. Chem. Rev.* **1998**, *178–180*, 427–505. (b) Akita, M.; Tanaka, Y.; Naitoh, C.; Ozawa, T.; Hayashi, N.; Takeshita, M.; Inagaki, A.; Chung, M.-C. Synthesis of a series of diiron complexes based on a tetraethynylethene skeleton and related C_6 -enediynyl spacers, (dppe)Cp*Fe–C≡CC(R)=C(R)C≡C–FeCp*-(dppe): tunable molecular wires. *Organometallics* **2006**, *25*, 5261–5275. (c) Tanaka, Y.; Inagaki, A.; Akita, M. A photoswitchable molecular wire with the dithienylethene (DTE) linker, (dppe)(η^5 -C₅Me₅)Fe–C≡C–DTE–C≡C–Fe(η^5 -C₅Me₅) (dppe). *Chem. Commun.* **2007**, 1169–1171. (d) Motoyama, K.; Koike, T.; Akita, M. Remarkable switching behavior of bimodally stimuli-responsive photochromic dithienylethenes with redox-active organometallic attachments. *Chem. Commun.* **2008**, 5812–5814. (e) Matsuura, Y.; Tanaka, Y.; Akita, M. *p*-Diethynylbenzene-based molecular wires, Fe–C≡C–*p*-C₆H₄–C≡C–Fe[Fe(η^5 -C₅Me₅) (dppe)]: Synthesis, 1041 substituent effects and unexpected formation of benzodifuran complex. *J. Organomet. Chem.* **2009**, *694*, 1840–1847. (f) Hatanaka, T.; Ohki, Y.; Kamachi, T.; Nakayama, T.; Yoshizawa, K.; Katada, M.; Tatsumi, K. Naphthalene and anthracene complexes sandwiched by two {(Cp*)-Fe^I} fragments: strong electronic coupling between the Fe^I centers. *Chem. - Asian J.* **2012**, *7*, 1231–1242. (g) Quardokus, R. C.; Lu, Y.; Wasio, N. A.; Lent, C. S.; Justaud, F.; Lapinte, C.; Kandel, S. A. Through-bond versus through-space coupling in mixed-valence molecules: observation of electron localization at the single-molecule scale. *J. Am. Chem. Soc.* **2012**, *134*, 1710–1714. (h) Ghazala, S. I.; Paul, F.; Toupet, L.; Roisnel, T.; Hapiot, P.; Lapinte, C. Di-organonon mixed valent complexes featuring “(η^2 -dppe)(η^5 -C₅Me₅)Fe” endgroups: smooth Class-III to Class-II transition induced by

- 1055 successive insertion of 1,4-phenylene units in a butadiyne-diyl bridge. *J.*
1056 *Am. Chem. Soc.* **2006**, *128*, 2463–2476.
- 1057 (20) Makhoul, R.; Sahnoun, H.; Dorcet, V.; Halet, J.-F.; Hamon, J.-
1058 R.; Lapinte, C. 1,2-diethynylbenzene-bridged $[\text{Cp}^*(\text{dppe})\text{Fe}]^{\text{III}}$ units:
1059 effect of steric hindrance on the chemical and physical properties.
1060 *Organometallics* **2015**, *34*, 3314–3326.
- 1061 (21) (a) Fox, M. A.; Le Guennic, B.; Roberts, R. L.; Brue, D. A.;
1062 Yufit, D. S.; Howard, J. A. K.; Manca, G.; Halet, J.-F.; Hartl, F.; Low, P.
1063 J. Simultaneous bridge-localized and mixed-valence character in
1064 diruthenium radical cations featuring diethynylaromatic bridging
1065 ligands. *J. Am. Chem. Soc.* **2011**, *133*, 18433–18446. (b) Bruce, M.
1066 L.; Low, P. J.; Hartl, F.; Humphrey, P. A.; de Montigny, F.; Jevric, M.;
1067 Lapinte, C.; Perkins, G. J.; Roberts, R. L.; Skelton, B. W.; White, A. H.
1068 Syntheses, structures, some reactions, and electrochemical oxidation of
1069 ferrocenylethynyl complexes of iron, ruthenium, and osmium.
1070 *Organometallics* **2005**, *24*, 5241–5255. (c) Bruce, M. I.; Burgun, A.;
1071 Fox, M. A.; Jevric, M.; Low, P. J.; Nicholson, B. K.; Parker, C. R.;
1072 Skelton, B. W.; White, A. H.; Zaitseva, N. N. Some ruthenium
1073 derivatives of penta-1, 4-diyne-3-one. *Organometallics* **2013**, *32*, 3286–
1074 3299. (d) Gao, L.-B.; Zhang, L.-Y.; Shi, L.-X.; Chen, Z.-N. Syntheses,
1075 characterization, redox properties, and mixed-valence chemistry of
1076 tetra- and hexanuclear diyndiyl complexes. *Organometallics* **2005**, *24*,
1077 1678–1684.
- 1078 (22) (a) Bruce, M. I.; Hall, B. C.; Kelly, B. D.; Low, P. J.; Skelton, B.
1079 W.; White, A. H. An efficient synthesis of polyyne and polyyndiyl
1080 complexes of ruthenium(II). *J. Chem. Soc., Dalton Trans.* **1999**, 3719–
1081 3728. (b) Bruce, M. I.; Ellis, B. G.; Gaudio, M.; Lapinte, C.; Melino,
1082 G.; Paul, F.; Skelton, B. W.; Smith, M. E.; Toupet, L.; White, A. H.
1083 Preparation, structures and some reactions of novel diyne complexes
1084 of iron and ruthenium. *Dalton Trans.* **2004**, 1601–1609.
- 1085 (23) (a) Paul, F.; Ellis, B. G.; Bruce, M. I.; Toupet, L.; Roisnel, T.;
1086 Costuas, K.; Halet, J.-F.; Lapinte, C. Bonding and substituent effects in
1087 electron-rich mononuclear ruthenium σ -arylacetylide of the formula
1088 $[(\eta^2\text{-dppe})(\eta^5\text{-C}_5\text{Me}_5)\text{Ru}(\text{C}\equiv\text{C})\text{-}1, 4\text{-}(\text{C}_6\text{H}_4\text{X})][\text{PF}_6]^n$ ($n = 0, 1$; X =
1089 NO_2 , CN, F, H, OMe, NH_2). *Organometallics* **2006**, *25*, 649–665.
1090 (b) Gendron, F.; Burgun, A.; Skelton, B. W.; White, A. H.; Roisnel, T.;
1091 Bruce, M. I.; Halet, J.-F.; Lapinte, C.; Costuas, K. Iron and ruthenium
1092 σ -polyyne of the general formula $\{[\text{M}(\text{dppe})\text{Cp}^*]\text{-}(\text{C}\equiv\text{C})_n\text{-R}\}^{0/+}$
1093 (M = Fe, Ru): an experimental and theoretical investigation.
1094 *Organometallics* **2012**, *31*, 6796–6811. (c) Bruce, M. I.; Costuas, K.;
1095 Davin, T.; Ellis, B. G.; Halet, J. F.; Lapinte, C.; Low, P. J.; Smith, M. E.;
1096 Skelton, B. W.; Toupet, L.; White, A. H. Iron versus Ruthenium:
1097 dramatic changes in electronic structure result from replacement of
1098 one Fe by Ru in $[\{\text{Cp}^*(\text{dppe})\text{Fe}\}\text{-C}\equiv\text{C}\text{-C}\equiv\text{C}\text{-}\{\text{Fe}(\text{dppe})\text{-}$
1099 $\text{Cp}^*\}]^{\text{II}}$ ($n = 0, 1, 2$). *Organometallics* **2005**, *24*, 3864–3881.
- 1100 (d) Gauthier, N.; Argouarch, G.; Paul, F.; Toupet, L.; Ladjarafi, A.;
1101 Costuas, K.; Halet, J.-F.; Samoc, M.; Cifuentes, M. P.; Corkery, T. C.;
1102 Humphrey, M. G. Electron-rich iron/ruthenium arylalkynyl complexes
1103 for third-order nonlinear optics: redox-switching between three states.
1104 *Chem. - Eur. J.* **2011**, *17*, 5561–5577. (e) Connelly, N. G.; Gamasa, M.
1105 P.; Gimeno, J.; Lapinte, C.; Lastra, E.; Maher, J. P.; Le Narvor, N.;
1106 Rieger, A. L.; Rieger, P. H. 17-Electron alkynyl complexes of
1107 cyclopentadienyliron(III). *J. Chem. Soc., Dalton Trans.* **1993**, 2575–
1108 2578. (f) Bruce, M. I.; Burgun, A.; Gendron, F.; Grelaud, G.; Halet, J.-
1109 F.; Skelton, B. W. Oxidative Dimerization of arylalkynyl–ruthenium
1110 complexes. *Organometallics* **2011**, *30*, 2861–2868. (g) Le Narvor, N.;
1111 Toupet, L.; Lapinte, C. Elemental carbon chain bridging two iron
1112 centers: syntheses and spectroscopic properties of $[\text{Cp}^*(\text{dppe})\text{Fe}\text{-}$
1113 $\text{C}_4\text{-FeCp}^*(\text{dppe})]^{\text{II}}$ $\bullet n[\text{PF}_6]^-$. X-ray crystal structure of the mixed
1114 valence complex ($n = 1$). *J. Am. Chem. Soc.* **1995**, *117*, 7129–7138.
1115 (h) Bruce, M. I.; Ellis, B. G.; Skelton, B. W.; White, A. H. Further
1116 reactions of some bis(vinylidene) diruthenium complexes. *J. Organo-*
1117 *met. Chem.* **2005**, *690*, 792–801.
- 1118 (24) (a) Grelaud, G.; Cifuentes, M. P.; Schwich, T.; Argouarch, G.;
1119 Petrie, S.; Stranger, R.; Paul, F.; Humphrey, M. G. Multistate redox-
1120 active metalated triarylamines. *Eur. J. Inorg. Chem.* **2012**, *2012*, 65–75.
1121 (b) Polit, W.; Exner, T.; Wuttke, E.; Winter, R. F. Vinylruthenium-
1122 triarylamine conjugates as electroswitchable polyelectrochromic NIR
1123 dyes. *BioInorg. React. Mech.* **2012**, *8*, 85–105.
- (25) (a) Costuas, K.; Cador, O.; Justaud, F.; Le Stang, S.; Paul, F.;
1124 Monari, A.; Evangelisti, S.; Toupet, L.; Lapinte, C.; Halet, J.-F. 3, 5-Bis
1125 (ethynyl) pyridine and 2, 6-bis(ethynyl) pyridine spanning two
1126 $\text{Fe}(\text{Cp}^*)(\text{dppe})$ units: role of the nitrogen atom on the electronic and
1127 magnetic couplings. *Inorg. Chem.* **2011**, *50*, 12601–12622. (b) Parthey,
1128 M.; Gluyas, J. B. G.; Schauer, P. A.; Yufit, D. S.; Howard, J. A. K.;
1129 Kaupp, M.; Low, P. J. Refining the interpretation of near-infrared band
1130 shapes in a polyyndiyl molecular wire. *Chem. - Eur. J.* **2013**, *19*, 9780–
1131 9784. (c) Parthey, M.; Kaupp, M. Quantum-chemical insights into
1132 mixed-valence systems: within and beyond the Robin–Day scheme.
1133 *Chem. Soc. Rev.* **2014**, *43*, 5067–5088. (d) Burgun, A.; Gendron, F.;
1134 Sumbly, C.; Roisnel, T.; Cador, O.; Costuas, K.; Halet, J.-F.; Bruce, M.
1135 I.; Lapinte, C. Hexatrienediyl chain spanning two $\text{Cp}^*(\text{dppe})\text{M}$
1136 termini (M = Fe, Ru): evidence for the dependence of electronic and
1137 magnetic couplings on the relative orientation of the termini.
1138 *Organometallics* **2014**, *33*, 2613–2627. (e) Makhoul, R.; Kumamoto,
1139 Y.; Miyazaki, A.; Justaud, F.; Gendron, F.; Halet, J.-F.; Hamon, J.-R.;
1140 Lapinte, C. Synthesis and properties of a mixed-valence compound
1141 with single-step tunneling and multiple-step hopping behavior. *Eur. J.*
1142 *Inorg. Chem.* **2014**, *2014*, 3899–3911. (f) Zhang, J.; Zhang, M.-X.; Sun,
1143 C.-F.; Xu, M.; Hartl, F.; Yin, J.; Yu, G.-A.; Rao, L.; Liu, S.-H.
1144 Diruthenium complexes with bridging diethynyl polyaromatic ligands:
1145 synthesis, spectroelectrochemistry, and theoretical calculations. *Orga-*
1146 *nometallics* **2015**, *34*, 3967–3978. (g) Denis, R.; Toupet, L.; Paul, F.;
1147 Lapinte, C. Electron-rich piano-stool iron σ -acetylides bearing a
1148 functional aryl group. synthesis and characterization of iron (II) and
1149 iron (III) complexes. *Organometallics* **2000**, *19*, 4240–4251.
- (26) (a) Gauthier, N.; Tchouar, N.; Justaud, F.; Argouarch, G.;
1151 Cifuentes, M. P.; Toupet, L.; Touchard, D.; Halet, J.-F.; Rigaut, S.;
1152 Humphrey, M. G.; Costuas, K.; Paul, F. Bonding and electron
1153 delocalization in ruthenium (III) σ -arylacetylide radicals $[\text{trans-Cl}(\eta^2\text{-}$
1154 $\text{dppe})_2\text{RuC}\equiv\text{C}(4\text{-C}_6\text{H}_4\text{X})]^+$ (X = NO_2 , C(O)H, C(O)Me, F, H,
1155 OMe, NMe₂): misleading aspects of the ESR anisotropy. *Organo-*
1156 *metallics* **2009**, *28*, 2253–2266. (b) Wuttke, E.; Pevny, F.; Hervault, Y.-
1157 M.; Norel, L.; Drescher, M.; Winter, R. F.; Rigaut, S. Fully delocalized
1158 (ethynyl) (vinyl) phenylene bridged triruthenium complexes in up to
1159 five different oxidation states. *Inorg. Chem.* **2012**, *51*, 1902–1915.
- (27) (a) Zhang, D.-B.; Wang, J.-Y.; Wen, H.-M.; Chen, Z.-N.
1161 Electrochemical, spectroscopic, and theoretical studies on diethynyl
1162 ligand bridged ruthenium complexes with 1, 3-bis(2-pyridylimino)
1163 isoindolate. *Organometallics* **2014**, *33*, 4738–4746. (b) Yao, C.-J.; Nie,
1164 H.-J.; Yang, W.-W.; Yao, J.; Zhong, Y.-W. Combined experimental and
1165 computational study of pyren-2,7-diyl-bridged diruthenium complexes
1166 with various terminal ligands. *Inorg. Chem.* **2015**, *54*, 4688–4698.
1167 (c) Fox, M. A.; Roberts, R. L.; Baines, T. E.; Le Guennic, B.; Halet, J.-
1168 F.; Hartl, F.; Yufit, D. S.; Albesa-Jové, D.; Howard, J. A. K.; Low, P. J.
1169 Ruthenium complexes of C,C'-bis(ethynyl) carboranes: an inves-
1170 tigation of electronic interactions mediated by spherical pseudo-
1171 aromatic spacers. *J. Am. Chem. Soc.* **2008**, *130*, 3566–3578.
1172 (28) (a) Zhang, J.; Ou, Y.-P.; Xu, M.; Sun, C.-F.; Yin, J.; Yu, G.-A.;
1173 Liu, S. H. Synthesis and characterization of dibenzoheterocycle-
1174 bridged dinuclear ruthenium alkynyl and vinyl complexes. *Eur. J. Inorg.*
1175 *Chem.* **2014**, *2014*, 2941–2951. (b) Khairul, W. M.; Fox, M. A.;
1176 Schauer, P. A.; Yufit, D. S.; Albesa-Jové, D.; Howard, J. A. K.; Low, P. J.
1177 The electronic structures of diruthenium complexes containing an
1178 oligo(phenylene ethynylene) bridging ligand, and some related
1179 molecular structures. *Dalton Trans.* **2010**, *39*, 11605–11615.
1180 (c) Armit, D. J.; Bruce, M. I.; Gaudio, M.; Zaitseva, N. N.; Skelton,
1181 B. W.; White, A. H.; Le Guennic, B.; Halet, J.-F.; Fox, M. A.; Roberts,
1182 R. L.; Hartl, F.; Low, P. J. Some transition metal complexes derived
1183 from mono- and di-ethynyl perfluorobenzenes. *Dalton Trans.* **2008**,
1184 6763–6775. (d) Klein, A.; Lavastre, O.; Fiedler, J. Role of the bridging
1185 arylethynyl ligand in Bi- and trinuclear ruthenium and iron complexes.
1186 *Organometallics* **2006**, *25*, 635–643.
1187 (29) Amthor, S.; Noller, B.; Lambert, C. UV/Vis/NIR spectral
1188 properties of triarylamines and their corresponding radical cations.
1189 *Chem. Phys.* **2005**, *316*, 141–152.
1190 (30) Weyland, T.; Ledoux, I.; Brasselet, S.; Zyss, J.; Lapinte, C.
1191 Nonlinear optical properties of redox-active mono-, bi-, and trimetallic
1192

- 1193 σ -acetylide complexes connected through a phenyl ring in the
1194 Cp*(dppe)Fe series. An example of electro-switchable NLO response.
1195 *Organometallics* **2000**, *19*, 5235–5237.
- 1196 (31) (a) Lambert, C.; Nöll, G. The class II/III transition in
1197 triarylamine redox systems. *J. Am. Chem. Soc.* **1999**, *121*, 8434–8442.
1198 (b) Cheng, H.-C.; Chiu, K. Y.; Lu, S. H.; Chen, C.-C.; Lee, Y. W.;
1199 Yang, T.-F.; Kuo, M. Y.; Chen, P. P.-Y.; Su, Y. O. Linear
1200 oligoarylamine: electrochemical, EPR, and computational studies of
1201 their oxidative states. *J. Phys. Chem. A* **2015**, *119*, 1933–1942.
- 1202 (32) (a) Parthey, M.; Gluyas, J. B. G.; Fox, M. A.; Low, P. J.; Kaupp,
1203 M. Mixed-valence ruthenium complexes rotating through a conforma-
1204 tional robin-day continuum. *Chem. - Eur. J.* **2014**, *20*, 6895–6908.
1205 (b) Marqués-González, S.; Parthey, M.; Yufit, D. S.; Howard, J. A. K.;
1206 Kaupp, M.; Low, P. J. Combined spectroscopic and quantum chemical
1207 study of [trans-Ru(C≡CC₆H₄R¹-4)₂(dppe)₂]ⁿ⁺ and [trans-Ru(C≡
1208 CC₆H₄R¹-4)(C≡CC₆H₄R²-4)(dppe)₂]ⁿ⁺ (n = 0, 1) complexes:
1209 interpretations beyond the lowest energy conformer paradigm.
1210 *Organometallics* **2014**, *33*, 4947–4963.
- 1211 (33) (a) Hush, N. S. Intervalence-transfer absorption. Part 2.
1212 Theoretical considerations and spectroscopic data. *Prog. Inorg. Chem.*
1213 **1967**, *8*, 391–444. (b) Hush, N. S. Distance dependence of electron
1214 transfer rates. *Coord. Chem. Rev.* **1985**, *64*, 135–157. (c) Hush, N. S.
1215 Homogeneous and heterogeneous optical and thermal electron
1216 transfer. *Electrochim. Acta* **1968**, *13*, 1005–1023.
- 1217 (34) (a) Hamon, P.; Justaud, F.; Cadore, O.; Hapiot, P.; Rigaut, S.;
1218 Toupet, L.; Ouahab, L.; Stueger, H.; Hamon, J.-R.; Lapinte, C. Redox-
1219 active organometallics: magnetic and electronic couplings through
1220 carbon-silicon hybrid molecular connectors. *J. Am. Chem. Soc.* **2008**,
1221 *130*, 17372–17383. (b) Paul, F.; Toupet, L.; Thépot, J.-Y.; Costuas,
1222 K.; Halet, J.-F.; Lapinte, C. Electron-rich piano-stool iron σ -acetylides.
1223 Electronic structures of arylalkynyl iron (III) radical cations.
1224 *Organometallics* **2005**, *24*, 5464–5478.
- 1225 (35) Shi, L. Q.; He, C.; Zhu, D. F.; He, Q. G.; Li, Y.; Chen, Y.; Sun,
1226 Y. X.; Fu, Y. Y.; Wen, D.; Cao, H. M.; Cheng, J. G. High performance
1227 aniline vapor detection based on multi-branched fluorescent triphenyl-
1228 amine-benzothiadiazole derivatives: branch effect and aggregation
1229 control of the sensing performance. *J. Mater. Chem.* **2012**, *22*, 11629–
1230 11635.
- 1231 (36) Sirohi, R.; Kim, D. H.; Yu, S.-C.; Lee, S. H. Novel di-anchoring
1232 dye for DSSC by bridging of two mono anchoring dye molecules: a
1233 conformational approach to reduce aggregation. *Dyes Pigm.* **2012**, *92*,
1234 1132–1137.
- 1235 (37) Bruce, M. I.; Ellis, B. G.; Low, P. J.; Skelton, B. W.; White, A. H.
1236 Syntheses, structures, and spectro-electrochemistry of {Cp*(PP)Ru}-
1237 C≡CC≡C{Ru(PP)Cp*}(PP = dppm, dppe) and their mono- and
1238 dications. *Organometallics* **2003**, *22*, 3184–3198.
- 1239 (38) Roger, C.; Hamon, P.; Toupet, L.; Rabaâ, H.; Saillard, J.-Y.;
1240 Hamon, J.-R.; Lapinte, C. Alkyl (pentamethylcyclopentadienyl)(1, 2-
1241 bis(diphenylphosphino)-ethane) iron (III) 17-electron complexes:
1242 synthesis, NMR and magnetic properties, and EHMO calculations.
1243 *Organometallics* **1991**, *10*, 1045–1054.
- 1244 (39) Fang, Z.; Samoc, M.; Webster, R. D.; Samoc, A.; Lai, Y. H.
1245 Triphenylamine derivatized phenylacetylene macrocycle with large
1246 two-photon absorption cross-section. *Tetrahedron Lett.* **2012**, *53*,
1247 4885–4888.
- 1248 (40) Sheldrick, G. M. *SHELXS-97, a Program for Crystal Structure*
1249 *Solution*; University of Göttingen: Göttingen, Germany, 1997.
- 1250 (41) Sheldrick, G. M. *SHELXL-97, a Program for Crystal Structure*
1251 *Refinement*; University of Göttingen, Göttingen, Germany, 1997.
- 1252 (42) Krejčík, M.; Daněk, M.; Hartl, F. Simple construction of an
1253 infrared optically transparent thin-layer electrochemical cell: Applica-
1254 tions to the redox reactions of ferrocene, Mn₂(CO)₁₀ and Mn(CO)₃
1255 (3,5-di-*t*-butyl-catecholate)⁻. *J. Electroanal. Chem. Interfacial Electro-*
1256 *chem.* **1991**, *317*, 179–187.
- 1257 (43) Frisch, M. J.; Trucks, G. W.; Schlegel, H. B.; Scuseria, G. E.;
1258 Robb, M. A.; Cheeseman, J. R.; Scalmani, G.; Barone, V.; Mennucci,
1259 B.; Petersson, G. A.; Nakatsuji, H.; Caricato, M.; Li, X.; Hratchian, H.
1260 P.; Izmaylov, A. F.; Bloino, J.; Zheng, G.; Sonnenberg, J. L.; Hada, M.;
1261 Ehara, M.; Toyota, K.; Fukuda, R.; Hasegawa, J.; Ishida, M.; Nakajima,
T.; Honda, Y.; Kitao, O.; Nakai, H.; Vreven, T.; Montgomery, J. A., Jr.;
Peralta, J. E.; Ogliaro, F.; Bearpark, M.; Heyd, J. J.; Brothers, E.; Kudin,
K. N.; Staroverov, V. N.; Kobayashi, R.; Normand, J.; Raghavachari, K.;
Rendell, A.; Burant, J. C.; Iyengar, S. S.; Tomasi, J.; Cossi, M.; Rega,
N.; Millam, J. M.; Klene, M.; Knox, J. E.; Cross, J. B.; Bakken, V.;
Adamo, C.; Jaramillo, J.; Gomperts, R.; Stratmann, R. E.; Yazyev, O.;
Austin, A. J.; Cammi, R.; Pomelli, C.; Ochterski, J. W.; Martin, R. L.;
Morokuma, K.; Zakrzewski, V. G.; Voth, G. A.; Salvador, P.;
Dannenberg, J. J.; Dapprich, S.; Daniels, A. D.; Farkas, Ö.;
Foresman, J. B.; Ortiz, J. V.; Cioslowski, J.; Fox, D. J. *Gaussian 09*,
Revision D.01; Gaussian, Inc.: Wallingford, CT, 2009.
- (44) Renz, M.; Theilacker, K.; Lambert, C.; Kaupp, M. A reliable
quantum-chemical protocol for the characterization of organic mixed-
valence compounds. *J. Am. Chem. Soc.* **2009**, *131*, 16292–16302.
- (45) (a) Cossi, M.; Rega, N.; Scalmani, G.; Barone, V. Energies,
structures, and electronic properties of molecules in solution with the
C-PCM solvation model. *J. Comput. Chem.* **2003**, *24*, 669–681.
(b) Barone, V.; Cossi, M. Quantum calculation of molecular energies
and energy gradients in solution by a conductor solvent model. *J. Phys.*
Chem. A **1998**, *102*, 1995–2001.